IEEE Access
Multidisciplinary | Rapid Review | Open Access Journal

Received November 29, 2020, accepted December 24, 2020, date of publication December 31, 2020,
date of current version January 11, 2021.

Digital Object Identifier 10.1109/ACCESS.2020.3048436

Cognitive UAV-Aided URLLC and mMTC Services: Analyzing Energy Efficiency and Latency

SAIFUR RAHMAN SABUJ[1], (Member, IEEE), AZMIR AHMED[2], YEONGI CHO[1], (Student Member, IEEE), KYOUNG-JAE LEE[1], (Senior Member, IEEE), AND HAN-SHIN JO[1], (Member, IEEE)

[1]Department of Electronics and Control Engineering, Hanbat National University, Daejeon 34158, South Korea
[2]Department of Electrical and Electronic Engineering, Brac University, Dhaka 1212, Bangladesh

Corresponding author: Han-Shin Jo (hsjo@hanbat.ac.kr)

This work was supported in part by the Korean Research Fellowship Program through the National Research Foundation of Korea (NRF) funded by the Ministry of Science and ICT (MSIT) under Grant 2019H1D3A1A01102869, and in part by the NRF grant funded by the Korea Government (MSIT) under Grant 2019R1A2C4070361.

ABSTRACT The integration of unmanned aerial vehicles (UAVs) into spectrum sensing cognitive communication networks can offer many benefits for massive connectivity services in 5G communications and beyond; hence, this work analyses the performance of non-orthogonal multiple access-based cognitive UAV-assisted ultra-reliable and low-latency communications (URLLCs) and massive machine-type communication (mMTC) services. An mMTC service requires better energy efficiency and connection probability, whereas a URLLC service requires minimising the latency. In particular, a cognitive UAV operates as an aerial secondary transmitter to a ground base station by sharing the unlicensed wireless spectrum. To address these issues, we derive the analytical expressions of throughput, energy efficiency, and latency for mMTC/URLLC-UAV device. We also formulate an optimisation problem of energy efficiency maximisation to satisfy the needs of URLLC latency and mMTC throughput and solve it using the Lagrangian method and the Karush–Kuhn–Tucker conditions. The algorithm is presented by jointly optimising the transmission powers of the mMTC and URLLC users. The derived expressions and algorithm are then used to evaluate the performance of the proposed system model. The numerical results show that the proposed algorithm improves the energy efficiency and satisfies the latency requirement of the mMTC/URLLC-UAV device.

INDEX TERMS Cognitive radio network, energy efficiency, finite information blocklength theory, Internet of Things, latency, massive machine-type communication, non-orthogonal multiple access, ultra-reliable and low-latency communications.

I. INTRODUCTION

In terms of the Internet of Things (IoT), the sixth-generation (6G) wireless network is designed to deal with the considerable increase in data traffic, connectivity, and services. Therefore, 6G is required to support several machines and sensors, referred to as machine-type communication (MTC) and cellular IoT. In the standardisation of a fifth-generation (5G) cellular system, MTC is classified into two types: critical MTC (cMTC) and massive MTC (mMTC) [1]. In 6G, cMTC focuses mainly on three modes of operation: (i) dependable cMTC, known as URLLC (e.g. autonomous driving), (ii) broadband cMTC (e.g. cloud gaming), and (iii) scalable cMTC (e.g. factory automation). On the other hand, mMTC focuses mainly on two operation modes: (i) globally scalable mMTC (e.g. non-terrestrial networks) and (ii) zero-energy mMTC (e.g. soil monitoring) [2]. The performance of MTC degrades in an overcrowded licensed spectrum. Hence, spectrum scarcity has become the biggest hindrance in 6G development.

Due to the rapid increase in wireless data traffic recently, unlicensed spectrum bands play a crucial role in a massive-scale and highly diverse MTC operation, as a way to aggregate additional bands and improve the capacity of future wireless systems [3]. The Third Generation Partnership Project (3GPP) introduced the new radio-based access to an unlicensed (NR-U) spectrum to provide an essential technology for supporting the future industry and society [4], [5].

The associate editor coordinating the review of this manuscript and approving it for publication was Quansheng Guan.

As part of an unlicensed activity, the long-term evolution (LTE) forum proposed to use an unlicensed band (LTE-U), providing an alternative solution for mitigating the bandwidth scarcity problem [6]. Therefore, spectrum sensing cognitive radio (CR) technology has been designed to access the unlicensed spectrum with the support of a large bandwidth [7].

3GPP has provided a fundamental guideline for establishing a steady and stable connection between unmanned aerial vehicles (UAVs) and existing cellular networks [8]. According to 3GPP, for maximum height and speed, a UAV requires values of 300 m and 44.44 m/s, respectively, in both urban and rural scenarios. According to [9], the communication link of a UAV can be classified into two categories: (i) control link (CL) and (ii) data link (DL). These communication links are briefly summarised as follows.

(i) CL: CL is known as a command-and-control (CaC) link, and is mainly used to avoid collision among UAVs. In addition, CL serves to command and control from the ground base station (BS) to UAVs, and updates the information from the UAV to the ground BS. Such information traffic is exact and rigid in cases of QoS, reliability, and latency. As CL depends on urgency, the latency requirement must be within 50 ms (single-way communication). Also, data rate should be 60-100 kbps for uplink and downlink transmissions.

(ii) DL: DL establishes communication among UAVs and communication that from UAVs to ground BS, or vice versa. DL is moderated QoS, which mainly depends on customer demands. The maximum data rate of DL for an uplink transmission is 50 Mbps.

From the above discussion, a UAV requires a highly reliable and low-latency communication-based CL for a safe and secure operation. Thus, a URLLC (dependable cMTC) service is essential for CL. DL is designed based on the UAV application. If a UAV is used for the time sensitivity of mission-critical applications, such as real-time tracking, quick transmission, autonomous driving, remote control, and tactile Internet, URLLC is prioritised for DL. On the other hand, if a UAV is used for sensing tasks, such as remote sensing, providing remote coverage, surveillance, security and observation, smart-monitoring in agricultural and civil infrastructural sectors, and environment monitoring, better energy efficiency and connection probability are required for DL. Therefore, mMTC is essential for DL. Depending on the nature of diverse communication requirements of diverse applications, DL is classified into two categories: URLLC and mMTC.

The energy consumption of a UAV as an aerial relay or BS is a major concern, because most UAVs use battery power to establish wireless communications, image processing and analysis, updating autonomous UAV operation, real-time piloting, flight authorisation, and navigation database updating and hovering [10]. A UAV consumes considerable power to run its mechanical function as well as for communication purposes, which degrades the endurance time and communication performance [11]. Therefore, an important downside of aerial BSs is their short lifetime, because of the battery consumption issue. Thus, it is essential for a UAV to consume energy efficiently, to increase the battery lifetime. For this purpose, an optimal power transmission schedule is required for efficient energy consumption while the UAVs are flying in a fixed route [12].

A. PRIOR STUDIES

Recently, different bodies from industry and academia have proposed to incorporate UAVs in 5G network. Li *et al.* (2018) conducted a complete survey for 5G and future 5G wireless networks based on UAV communication. Moreover, not only various UAV-based 5G techniques but also space-air-ground integrated networks and related research challenges are being investigated [13]. Another comprehensive study was conducted by Fotouhi *et al.* (2019), where potential roles of a UAV within cellular networks, 3GPP developments for serving aerial users, and new regulations were developed for the commercial use of UAVs; moreover, most advanced UAV prototyping was elaborately discussed [12]. Ernest *et al.* (2020) surveyed both analytical and open research problems for enhancing the spectrum efficiency and discussing the interference management scheme for a hybrid duplex-UAV communication system (HBD-UCS). In addition, they illustrated the non-orthogonal multiple access (NOMA) technique for a multi-UAV HBD-UCS where they presented a signal model for the mentioned communication system [14]. Sharma *et al.* (2017) studied an energy-efficient scheme that utilises UAVs to discover devices in 5G-enabled IoT and body sensor networks [15]. Moreover, Ding *et al.* (2018) conducted a brief survey containing state-of-the-art studies on an amateur drone surveillance scheme incorporated with cognitive IoT, where they introduced a perception known as Dragnet by adapting the most recently developed cognitive IoT scheme [16].

Liu *et al.* (2020) proposed a UAV-empowered data-collecting network model exhibiting the wireless energy transfer (WET) feature, which allows the UAV to supply power to IoT devices, and formulated two allocation schemes for the optimal power of data transmission and WET time [17]. B. Ji *et al.* (2020) investigated a cooperative secrecy transmission scheme to use decode-and-forward UAV selection with energy harvesting technique in the underlying CR network [18]. Mu *et al.* (2020) investigated the ground aerial uplink NOMA cellular network problems to reduce the time required by a UAV to complete its mission, proposing the graph and topology theories as prominent solutions for analyzing the feasibility of the formulated problems. Moreover, they provided a solution using graph theory that obeyed the fly-hover-fly policy, whereas the successive convex approximation (SCA) technique ensured the solution for the local suboptimal problem [19]. Zhang *et al.* (2020) proposed a multi-UAV-assisted multi-access edge computing scheme integrated with NOMA to solve the high-energy-consumption and computation capacity problems.

Additionally, they used SCA and quadratic approximation techniques to evaluate the optimal problems and formulated an algorithm for obtaining an optimal solution [20].

Liu *et al.* (2020) studied a clustering cognitive IoT network integrated with the NOMA scheme to increase the transmission performance by reducing interference caused to primary users, and introduced a clustering algorithm to identify the cluster node and select a cluster head; the cluster head substitution also occurred during the transmission period to bypass the energy consumption of each cluster head [21]. Mozaffari *et al.* (2016) studied not only an ideal trajectory and deployment of UAVs but also an ideal clustering of IoT devices, to aggregate the data by using minimum power transmitted from the ground-located IoT devices [22]. Liu *et al.* (2019) introduced a distributed NOMA system in a heterogeneous IoT network for a UAV-enabled emergency communication scheme, by using the multi-objective resource allocation technique [23]. Almasoud *et al.* (2019) investigated a cognitive UAV network to circulate data to IoT devices, and formulated a problem in the mixed-integer nonlinear program that dealt with the maximisation of the minimum number of bits obtained by IoT devices [24]. Hattab *et al.* (2020) indicated that UAVs are used as a data collector for both cellular users, and that several IoT devices share the same spectrum. Moreover, they formulated an optimisation problem to maximise the energy efficiency of an IoT device by optimising its minimum transmit power [25].

Hu *et al.* (2020) suggested a UAV-enabled ground wireless network where two transmission systems, including relaying and NOMA, were proposed. In addition, they presented infinite blocklength (IBL) and finite blocklength (FBL) codes, and proposed an optimal resource allocation technique for the relaying and NOMA systems to improve the UAV throughput while maintaining the QoS for the ground user [26]. She *et al.* (2019) presented a URLLC-enabled UAV communication scheme containing a control and non-payload communication (CNPC) channel, where they optimised the UAV height, antenna configuration, and the period of the uplink and downlink transmission state to enhance the CNPC link between the UAV and ground control station. Moreover, they formulated an algorithm as a promising solution for the optimisation problem [27]. Pan *et al.* (2019) investigated the joint blocklength and location optimisation problem for a UAV-assisted relay scheme that satisfied the URLLC conditions. Moreover, they formulated an algorithm as a solution for the optimisation problem, where a perturbation-based iterative algorithm was proposed [28]. Han *et al.* (2019) proposed a UAV-enabled URLLC scheme integrated with NOMA transmission, suggesting the optimisation of the number of user groups and the beamwidth for reducing the block error probability. Moreover, for user grouping, they formulated the K-means algorithm and extended affinity propagation algorithm [29]. Ren *et al.* (2019) studied the average achievable data rate (AADR) from a ground control station (GCS) for a UAV network, where the URLLC scheme is mandatory for mitigating collision. Moreover, after formulating the approximate AADR by using the Gaussian-Chebyshev quadrature method, they extracted the closed-form AADR [30]. Chu *et al.* (2019) studied the UAV-assisted cognitive IoT networks, maximising the minimal average rate for the secondary network [31].

B. SCOPE AND CONTRIBUTIONS

The aforementioned previous studies [17]–[25] on UAV communication were conducted under the assumption of the IBL scheme (i.e. Shannon's capacity). However, for the stringent latency and reliability requirements between UAV and ground user, the conventional IBL scheme is no longer applicable. To tackle this problem, an FBL information theoretic model was developed in [26]–[31]. Using this model, several studies have been conducted on UAV throughput [26], available range of the CNPC link [27], decoding error probability [28], block error probability [29], and data rate [30], [31]. Only the aforementioned study [31] considered the performance of a UAV-aided CR network; however, it did not assume the NOMA system. Thus, in the present study, we consider the performance modelling and optimisation of a cognitive UAV with NOMA for supporting joint mMTC and URLLC transmission. This UAV is called mMTC/URLLC-UAV hereafter. The contributions of this study are as follows:

1) We propose an energy-efficient and low-latency mMTC/URLLC-UAV network. For this network, we obtain an analytical expression of throughput for the mMTC/URLLC-UAV device using the FBL information theoretic model.
2) Following the throughput characterisations, we derive the energy efficiency expressions for the mMTC/URLLC-UAV device. In addition, we obtain an analytical expression of latency for the mMTC/URLLC-UAV device.
3) Finally, we formulate an optimisation problem with the objective of maximising the energy efficiency of mMTC/URLLC-UAV and satisfying a latency constraint by joint optimising the transmission powers allocated to URLLC and mMTC. The optimisation problem is shown to be non-convex depending on the system parameters, such as transmission power, channel gain, and noise power. To solve the formulated problem, the Lagrangian approach and the Karush–Kuhn–Tucker (KKT) conditions are applied.

C. ORGANISATION

The rest of this paper is structured as follows. Section II presents the system model, including the network model, frame structure, channel model, UAV energy consumption model, and latency. In section III, we derive the performance metrics, such as throughput, energy efficiency, and latency of mMTC/URLLC-UAV device. In section IV, the optimisation problem is formulated and solved for mMTC/URLLC-UAV device. In Section V, numerical results are presented, and finally, we conclude the study in Section VI.

II. SYSTEM MODEL AND ASSUMPTIONS

A. NETWORK DESCRIPTION

Fig. 1 shows a cognitive UAV-aided network model, which comprises a next-generation base station (gNB), an mMTC/URLLC-UAV, and a primary transmitter (PT). We consider that mMTC/URLLC-UAV and gNB are secondary nodes equipped with a single antenna. In this model, the PT and gNB are installed on the ground, while mMTC/URLLC-UAV is installed in the air. We assume that the mMTC/URLLC-UAV device first senses the mMTC user data equipped with on-board sensors, and then transmits a signal from the mMTC/URLLC-UAV to gNB. Also, the mMTC/URLLC-UAV device sends its emergency information, such as CaC data or their current operation states, to gNB. In such network, the uplink (mMTC data sensing) and downlink (mMTC[1] and URLLC[2] users' data delivery) transmissions use different spectral resource blocks. In this paper, we only focus on the downlink transmission of mMTC/URLLC-UAV device (i.e., from mMTC/URLLC-UAV to gNB) to share the same spectral resource block. To enable the coexistence of mMTC and URLLC users' data in the same device, the NOMA scheme can be used because of sharing the entire time and frequency resources for mMTC and URLLC users' data by superimposing their signals only with different power levels. Throughout this paper, T_{sm}/T_{su} represents a secondary mMTC/URLLC-UAV transmitter, R_{sg} represents a secondary gNB receiver, and T_p represents a PT.

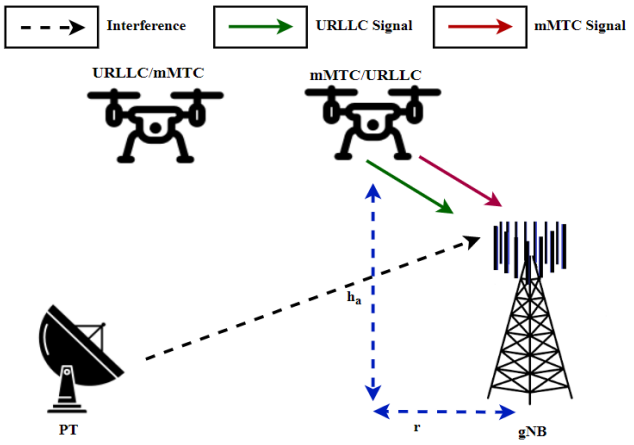

FIGURE 1. An example of UAV-aided network coexisting with URLLC and mMTC users sharing the same resource block where only interference comes from PT. Due to the considered NOMA system model, different power levels for URLLC and mMTC users are allocated.

B. FRAME STRUCTURE

In the same time and frequency domains, it is difficult to accommodate two users, such as URLLC and mMTC users. Two users share the same radio resource blocks, where each resource block comprises a single frequency channel and a single timeslot, as shown in Fig. 2. Due to the reliable communication, the NOMA technique is applied among the users so that URLLC and mMTC users can use the same frequency and timeslot but in different power levels. Several user signals are classified using the successive interference cancellation (SIC) scheme, though they are using the same resource block [32].

[1]Sensing data delivery
[2]CaC data delivery

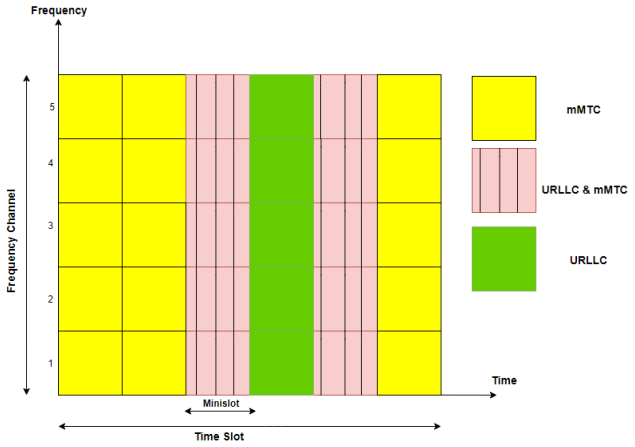

FIGURE 2. Illustration of the time-frequency resource allocation for URLLC and mMTC users.

In each minislot, T_{sm}/T_{su} seeks the occupied and unoccupied resource blocks from the unlicensed spectrum prior to transmission at the beginning. Typically, T_p forwards its ordinary data to the assigned primary receiver as well. T_{sm}/T_{su} is used to calculate the signal-to-noise ratio (SNR) of T_p. Consequently, the received SNR at T_{sm}/T_{su} is compared with the predefined SNR. The resource block is identified as occupied only when the received SNR is greater than the predefined SNR; otherwise, it is considered as unoccupied. The theoretical term $\Omega(\gamma_p)$ is defined as [33]

$$\Omega(\gamma_p) = \begin{cases} 1, & \gamma_p \geq \gamma_t \\ 0, & \gamma_p < \gamma_t, \end{cases} \tag{1}$$

where γ_p is the SNR of T_p and γ_t is the predefined SNR.

Based on the results of the spectrum sensing period, T_{sm}/T_{su} is used as the unoccupied resource block in transmission.

C. THREE-DIMENSIONAL CHANNEL MODEL

A three-dimensional (3D) channel model is presented here. Let us assume that a cognitive UAV flies at a constant height of h_a. Hence, it is assumed that the small-scale fading caused by Doppler spread is independent and identically distributed (i.i.d.) while the transmission is on-going. Thus, a combination of pathloss and fast fading in the channel gain can be described as [34], [35]

$$g_{xy}\left(h_a, r_{xy}\right) = \frac{\tilde{g}_{xy}}{\sqrt{PL_{xy}\left(h_a, r_{xy}\right)}}, \tag{2}$$

where x and y are two different nodes in the ground. r_{xy} is the horizontal distance between x and y, which is $\sqrt{(x_i - x_j)^2 + (y_i - y_j)^2}$. $PL_{xy}(h_a, r_{xy})$ is the pathloss between x and y, which is isolated by distance r_{xy} with height h_a. $\tilde{g}_{xy}$ is the fast fading channel gain, and is given by

$$\tilde{g}_{xy} = \sqrt{\frac{\mathcal{K}}{1+\mathcal{K}}}\tilde{g}_L + \sqrt{\frac{1}{1+\mathcal{K}}}\tilde{g}_N, \tag{3}$$

where $\tilde{g}_{xy}$ is a combination of line-of-sight (LoS) and non-line-of-sight (NLoS) components, $\tilde{g}_L$ represents an LoS channel component with $|\tilde{g}_L| = 1$, and $\tilde{g}_N$ denotes a random scattered component that is a random variable with a zero mean and unit variance. $\mathcal{K}$ denotes the Rician factor.

Three types of communication links are involved in a cognitive UAV network. First, the link between the air (T_{sm}/T_{su}) and ground (R_{sg}) is denoted as A-t-G and that between the air (T_{sm}/T_{su}) and air (T_{sm}/T_{su}) is denoted as A-t-A. In addition, the ground (T_p/R_{sg}) to ground (R_{sg}/T_p) link is labelled as G-t-G. In this paper, we discuss two types of channels: A-t-G channel and G-t-G channel.

1) A-T-G CHANNEL

In A-t-G, both the non-fading LoS component and fading NLoS component are present. It is assumed that LoS links T_{sm}/T_{su} and R_{sg} with a particular probability of p_{xy}^L. In [36], the probability of LoS for the A-t-G link is provided as follows:

$$p_{xy}^L(h_a, r_{xy}) = \frac{1}{1 + \Phi \exp\left(-\varphi\left[\tan^{-1}\left(\frac{h_a}{r_{xy}}\right) - \Phi\right]\right)}, \tag{4}$$

where Φ and φ are the constant parameters related to the environment characteristics. This implies that various environmental conditions, such as rural, urban, and dense urban, are used to determine the constant values Φ and φ. Therefore, the A-t-G pathloss in decibel (dB) is represented as

$$PL_{xy}(h_a, r_{xy}) = 20\log_{10}\left(\frac{4\pi f\sqrt{h_a^2 + r_{xy}^2}}{c}\right) + \upsilon_1, \tag{5}$$

where $\upsilon_1 = p_{xy}^L L_L + (1 - p_{xy}^L)L_N$, f indicates the carrier frequency (in Hz), and c indicates the speed of light (in m/s). In addition, L_L and L_N indicate the additional loss caused by the LoS and NLoS links.

Due to the considered communication scenario, A-t-G channel is generated by substituting (3), (4), and (5) into (2).

2) G-T-G CHANNEL

In G-t-G, only NLoS is assumed to be present, because of the ground nodes. Therefore, the NLoS pathloss in dB is calculated as

$$PL_{xy}(h_a, r_{xy}) = 20\log_{10}\left(\frac{4\pi f\sqrt{h_a^2 + r_{xy}^2}}{c}\right) + L_N. \tag{6}$$

Due to the considered communication scenario, G-t-G channel is generated by substituting (3) and (6) into (2).

D. UAV ENERGY CONSUMPTION MODEL

Most commercial UAVs use rechargeable batteries, and some large UAVs use fuel, such as gas duration of a long flight [12]. In addition, applying solar energy or wind energy to provide power to UAVs is a promising technique [11]. A power supply unit is required to operate the UAV and its on-board communication equipment. Mainly, two types of power are required: mechanical hover power, when the UAV is moving in the sky, and operational power, for particular tasks such as information processing, power transmission, and circuits power (transceiver and amplifier). In [37], the expression of propulsion power consumption of UAV in the hovering state P_{hov} can be expressed as

$$P_{hov} = \frac{\delta}{8}\rho s A_d v_a^3 r^3 + (1+\eta)\sqrt{\frac{(mg)^3}{2\rho A_d}}, \tag{7}$$

where δ, ρ, s, A_d, v_a, r, η, m, and g are the profile drag coefficient, air density (in kg/m^3), rotor solidity, rotor disc area (in m^2), blade angular velocity (in rad/s), rotor radius (in m), incremental correctional factor of induced power, mass of the UAV (in kg), gravity of Earth (in m/s^2), respectively. Furthermore, the weight of UAV can be calculated as $W = mg$ (in N).

From (7), the amount of energy consumed by the UAV to operate hovering for time t_h can be expressed as

$$E_{uav} = P_{hov} t_h. \tag{8}$$

According to (8), the UAV has to consume energy for hovering without information transmission. Thus, the expression of total energy consumption during information transmission can be defined as

$$E_{uavT} = P_{hov} t_h + P_d t_d + E_c, \tag{9}$$

where P_d and t_d denote the transmission power and period, respectively; and E_c denotes constant energy consumption due to spectrum sensing, information processing, encoding, and decoding.

E. PHYSICAL LAYER LATENCY

To communicate with and control the UAV in a reliable manner, latency is a big issue in a cognitive UAV network. The physical layer latency of one-way transmission (T_L) is the time taken for the transmission of information from the source node (transmitter) to the destination node (receiver) [38]. As shown in Fig. 3, it can be divided into the following six parts:

$$t_L = t_s + t_{pre} + t_{en} + t_t + t_{prop} + t_{de}, \tag{10}$$

where t_s is the spectrum sensing time for determining the idle resource block in the unlicensed spectrum. t_{pre} is the pre-processing time required for the information exchange (e.g., connection request, scheduling grant, channel training and feedback, and queuing delay). t_{en} is the information encoding time. t_t is the transmission time of a piece of information. t_{prop} is the information propagation time between the

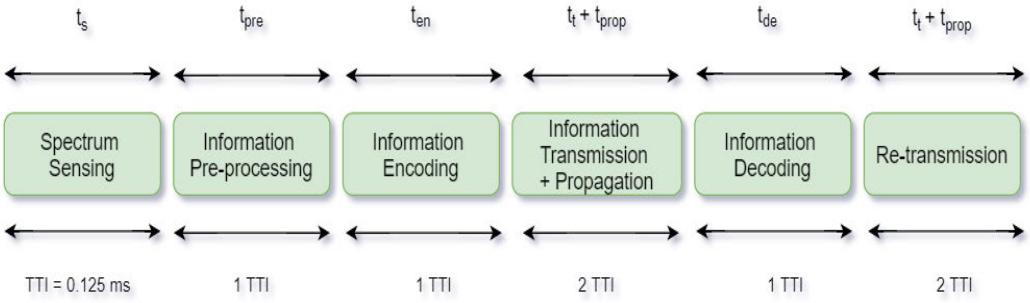

FIGURE 3. Illustrations of latency period of one ms for unlicensed spectrum.

transmitter and receiver, and t_{de} is the information decoding time. According to 5G and beyond, the latency budget has been proposed as one millisecond (ms); thus, one transmission time interval (TTI) is equal to 0.125 ms, as shown in Fig. 3.

III. MATHEMATICAL MODEL

In this section, we provide analytical expressions for the throughput, energy efficiency, and latency for T_{sm}/T_{su} device in our proposed system model.

A. SINR ANALYSIS

For the considered network, the signal-to-interference-plus-noise ratio (SINR) at R_{sg} from T_{sm}/T_{su} can be defined as

$$\text{SINR}_{u\to g} = \frac{\mathcal{P}_u \left|g_{ug}\right|^2}{\sigma^2 + \mathcal{P}_m \left|g_{ug}\right|^2 + \mathcal{P}_p \left|g_{pg}\right|^2}, \quad (11)$$

$$\text{SINR}_{m\to g} = \frac{\mathcal{P}_m \left|g_{ug}\right|^2}{\sigma^2 + \Theta\mathcal{P}_u \left|g_{ug}\right|^2 + \mathcal{P}_p \left|g_{pg}\right|^2}, \quad (12)$$

where $\mathcal{P}_u > \mathcal{P}_m$. $\mathcal{P}_u$, $\mathcal{P}_m$, and $\mathcal{P}_p$ are the transmit power of T_{su}, T_{sm}, and T_p, respectively. g_{ug} is the channel gain between T_{sm}/T_{su} and R_{sg}. g_{pg} is the channel gain between T_p and R_{sg}. σ^2 is the noise power. Θ represents an imperfect SIC coefficient. A natural SIC strategy is to first decode URLLC data and then decode mMTC data. In a real environment, a perfect SIC decoding is complicated to be achieved, because of error propagation when decoding the signal of NOMA users [39], [40]. Therefore, it is necessary to study the NOMA system under the imperfect SIC condition. In the presence of an imperfect SIC, the SIC coefficient varies from 0 to 1 ($0 < \Theta < 1$), where $\Theta = 0$ and $\Theta = 1$ represent the perfection and absence of SIC, respectively.

B. THROUGHPUT ANALYSIS

Throughput is defined as the transmission speed from the source node (transmitter) to the destination node (receiver), or vice versa (in *bps*). The mathematical expressions of throughput for mMTC/URLLC-UAV device is provided below:

1) EFFECTIVE THROUGHPUT

A cognitive UAV originally identifies the existence or non-existence of T_p in our suggested model. We apply Ω as a marker to differentiate the status of T_p. $\Omega = 1$ implies that T_p is progressive (present) in the transmission, while $\Omega = 0$ implies that T_p is unprogressive (absent) in the transmission. The effective throughput for T_{su} when $\Omega = 0$ can be formulated as

$$ED_u = \frac{t_t}{t_s + t_t} p_r\left(\Omega = 0\right)\left(1 - p_f\right) \cdot \left[\mathcal{B}\log_2\left(1 + \upsilon_1\right) - \sqrt{\frac{\upsilon_2}{C_b}} Q^{-1}(\varepsilon)\right], \quad (13)$$

where $\upsilon_1 = \frac{\mathcal{P}_u |g_{ug}|^2}{\sigma^2 + \mathcal{P}_m |g_{ug}|^2}$, $\sigma^2 = N_o\mathcal{B}$, and $\upsilon_2 = 1 - (1+\upsilon_1)^{-2}$. υ_1 is the SINR as given in (11) consideration of $\mathcal{P}_p = 0$. N_o is the noise power spectral density. $\mathcal{B}$ is the bandwidth of the resource block. C_b and ε represent the channel blocklength and probability of decoding error, respectively. $Q^{-1}(\cdot)$ is the inverse of Q-function. t_t and t_s represent transmission time and sensing time, respectively. The term $p_r\left(\Omega = 0\right)\left(1 - p_f\right)$ is the correct detection probability when T_p is not present, and p_f indicates the probability of a false alarm. The proof of (13) is provided in **Appendix A**.

Following a similar analysis for T_{su}, an effective throughput for T_{sm} when $\Omega = 0$ can be formulated as

$$ED_m = \frac{t_t}{t_s + t_t} p_r\left(\Omega = 0\right)\left(1 - p_f\right) \cdot \cdot \left[\mathcal{B}\log_2\left(1 + \upsilon_5\right) - \sqrt{\frac{\upsilon_6}{C_b}} Q^{-1}(\varepsilon)\right], \quad (14)$$

where $\upsilon_5 = \frac{\mathcal{P}_m |g_{ug}|^2}{\sigma^2 + \Theta\mathcal{P}_u |g_{ug}|^2}$ and $\upsilon_6 = 1 - (1+\upsilon_5)^{-2}$. υ_5 is the SINR as given in (12) consideration of $\mathcal{P}_p = 0$. The proof of (14) is provided in **Appendix A**.

The system effective throughput when $\Omega = 0$ can be expressed as

$$ED_{um} = ED_u + ED_m. \quad (15)$$

2) INTERFERENCE THROUGHPUT

In order to interfere from T_p, the interference throughput for T_{su} when $\Omega = 1$ is represented as

$$ID_u = \frac{t_t}{t_s + t_t} p_r\,(\Omega = 1)\,(1 - p_d) \cdot \left[\mathcal{B}\log_2\,(1 + \upsilon_3) - \sqrt{\frac{\upsilon_4}{C_b}} Q^{-1}(\varepsilon)\right], \quad (16)$$

where $\upsilon_3 = \frac{\mathcal{P}_u |g_{ug}|^2}{\sigma^2 + \mathcal{P}_m |g_{ug}|^2 + \mathcal{P}_p |g_{pg}|^2}$ and $\upsilon_4 = 1 - (1 + \upsilon_3)^{-2}$. $p_r\,(\Omega = 1) = 1 - p_r\,(\Omega = 0)$. υ_3 is the SINR as given in (11). The term $p_r\,(\Omega = 1)\,(1 - p_d)$ is an incorrect detection probability when T_p is present, and p_d indicates the detection probability. The proof of (16) is provided in **Appendix A**.

In addition, the interference throughput for T_{sm} when $\Omega = 1$ can be formulated as

$$ID_m = \frac{t_t}{t_s + t_t} p_r\,(\Omega = 1)\,(1 - p_d) \cdot \left[\mathcal{B}\log_2\,(1 + \upsilon_7) - \sqrt{\frac{\upsilon_8}{C_b}} Q^{-1}(\varepsilon)\right], \quad (17)$$

where $\upsilon_7 = \frac{\mathcal{P}_m |g_{ug}|^2}{\sigma^2 + \Theta\mathcal{P}_u |g_{ug}|^2 + \mathcal{P}_p |g_{pg}|^2}$ and $\upsilon_8 = 1 - (1 + \upsilon_7)^{-2}$. υ_7 is the SINR as given in (12). The proof of (17) is provided in **Appendix A**.

The system interference throughput when $\Omega = 1$ can be expressed as

$$ID_{um} = ID_u + ID_m. \quad (18)$$

C. ENERGY EFFICIENCY ANALYSIS

In our considered system, energy efficiency is defined as the ratio of system throughput to the total power consumed by the device, for example, mMTC/URLLC-UAV and gNB devices. The energy efficiency for T_{sm}/T_{su} can be expressed in terms of system effective throughput and system interference throughput as

$$EE_{muE} = \frac{ED_{um}}{P_{hov} + \mathcal{P}_u + \mathcal{P}_m + \mathbb{P}_c}, \quad (19)$$

$$EE_{muI} = \frac{ID_{um}}{P_{hov} + \mathcal{P}_u + \mathcal{P}_m + \mathbb{P}_c}, \quad (20)$$

where $\mathbb{P}_c$ is the constant power consumption due to the spectrum sensing, information processing, encoding, and decoding. P_{hov} is the propulsion power consumption of UAV in the hovering state as given in (7).

D. LATENCY ANALYSIS

In this subsection, we analyse the latency of mMTC/URLLC-UAV. From the definition in (10), each device completes the task within limited time (t_{LT}). Thus, each T_{sm}/T_{su} completes the specific task within t_{LT}. The system latency for T_{sm}/T_{su} device can be expressed as

$$t_s + t_{pre} + t_{en} + 2t_t + 2t_{prop} + t_{de} \leq t_{LT}. \quad (21)$$

Substituting the value of TTI $=$ 0.125 ms, the system latency for T_{sm}/T_{su} device expression can be simplified as

$$t_{prop} \leq \mathbb{T}_c, \quad (22)$$

where $\mathbb{T}_c = 0.125$ ms.

Due to the communication between T_{sm}/T_{su} and R_{sg}, the propagation time for effective and interference cases can be expressed as

$$t_{propE} = \frac{N_b}{ED_u}, \quad (23)$$

$$t_{propI} = \frac{N_b}{ID_u}, \quad (24)$$

where N_b is the number of bits transmitted. We consider only URLLC latency because a natural SIC strategy is to first decode the URLLC data and then decode mMTC data.

IV. ENERGY EFFICIENCY MAXIMISATION

In this section, we analyse the optimisation problem of energy efficiency for an mMTC/URLLC-UAV device. We assume the two energy efficiency cases, with the presence and absence of interference. Our objective is to maximise T_{sm}/T_{su} energy efficiency by jointly optimising the transmission power of T_{su} and T_{sm} under the transmit power constraint, the SINR constraint of T_{su} and T_{sm} for latency and throughput requirement. Thus, we obtain the expression of optimal power for T_{su} and T_{sm}. The optimisation problems of energy efficiency for the two cases are described below:

A. EFFECTIVE CASE

For the effective case (19), we aim to maximise the energy efficiency of T_{sm}/T_{su}. The observation of (19) clearly shows that the energy efficiency of T_{sm}/T_{su} is the required maximum value. Thus, it is a single-objective optimisation problem (SOP) and can be formulated as

$$\mathrm{P1}_1 : \max_{\mathcal{P}_u, \mathcal{P}_m} EE_{muE}(\mathcal{P}_u, \mathcal{P}_m) \quad (25a)$$

$$\text{s.t. } \mathcal{P}_u + \mathcal{P}_m \leq \mathcal{P}_t, \quad (25b)$$

$$\frac{\mathcal{P}_u |g_{ug}|^2}{\sigma^2 + \mathcal{P}_m |g_{ug}|^2} \geq \upsilon_u, \quad (25c)$$

$$\frac{\mathcal{P}_m |g_{ug}|^2}{\sigma^2 + \Theta\mathcal{P}_u |g_{ug}|^2} \geq \upsilon_m, \quad (25d)$$

$$\upsilon_u \geq \upsilon_m, \quad (25e)$$

where $\mathcal{P}_t$ is the total power budget. υ_u and υ_m are the minimum SINR of T_{su} and T_{sm}. (25a) denotes the energy efficiency of T_{sm}/T_{su} for the effective case discussed in Section III.C, (25b) represents the total power constraint of T_{su}/T_{sm}, (25c) represents the SINR constraint of T_{su} for satisfying URLLC latency requirement given in (22), and (25d) represents the SINR constraint of T_{sm} for satisfying the minimum required throughput given in (14). After some

manipulations of (25c) and (25d), we obtain a SOP as

$$\mathrm{P1}_2: \max_{\mathcal{P}_u,\mathcal{P}_m} EE_{muE}(\mathcal{P}_u,\mathcal{P}_m) \tag{26a}$$
$$\text{s.t. } \mathcal{P}_u+\mathcal{P}_m \le \mathcal{P}_t, \tag{26b}$$
$$\mathcal{P}_u \ge \upsilon_u\left(\sigma^2+\mathcal{P}_m\left|g_{ug}\right|^2\right)/\left|g_{ug}\right|^2, \tag{26c}$$
$$\mathcal{P}_u \le (\mathcal{P}_m/\Theta\upsilon_m)-\left(\sigma^2/\Theta\left|g_{ug}\right|^2\right), \tag{26d}$$
$$\upsilon_u \ge \upsilon_m, \tag{26e}$$

The objective function (26a) is non-convex depending on variables such as $\mathcal{P}_u$, $\mathcal{P}_m$, g_{ug}, and σ^2. The constraints (26b), (26c), and (26d) are a linear function with respect to (w.r.t.) $\mathcal{P}_u$ and $\mathcal{P}_m$. Thus, problem ($\mathrm{P1}_2$) is a non-convex optimisation problem depending on the variables.

Theorem 1: The optimal solutions of the optimisation problem in ($P1_2$) with the objective in (26a) and constraints in (26b - 26e) are given by

$$\mathcal{P}_u^* = \max\left(\mathcal{P}_{u1},\mathcal{P}_{u2}\right), \tag{27}$$
$$\mathcal{P}_m^* = \mathcal{P}_t-\mathcal{P}_u^*, \tag{28}$$

where $\mathcal{P}_{u1} = \frac{\upsilon_u}{1+\upsilon_u}\left[\mathcal{P}_t+\frac{\sigma^2}{|g_{ug}|^2}\right]$ and $\mathcal{P}_{u2} = \frac{\upsilon_m}{1+\Theta\upsilon_m}\left[\frac{\mathcal{P}_t}{\upsilon_m}-\frac{\sigma^2}{|g_{ug}|^2}\right]$.

Proof: The proof is provided in **Appendix B**.

B. INTERFERENCE CASE

Similar to effective case, the SOP for the interference case (20) is mathematically represented as

$$\mathrm{P2}_1: \max_{\mathcal{P}_u,\mathcal{P}_m} EE_{muI}(\mathcal{P}_u,\mathcal{P}_m) \tag{29a}$$
$$\text{s.t. } \mathcal{P}_u+\mathcal{P}_m \le \mathcal{P}_t, \tag{29b}$$
$$\mathcal{P}_u \ge \upsilon_u\left(\sigma^2+\mathcal{P}_m\left|g_{ug}\right|^2\right)/\left|g_{ug}\right|^2, \tag{29c}$$
$$\mathcal{P}_u \le (\mathcal{P}_m/\Theta\upsilon_m)-\left(\sigma^2/\Theta\left|g_{ug}\right|^2\right), \tag{29d}$$
$$\upsilon_u \ge \upsilon_m, \tag{29e}$$

where (29a) denotes the energy efficiency of T_{sm}/T_{su} for the interference case discussed in Section III.C. The objective function (29a) is proportional to interference throughput (18). As shown in problem ($\mathrm{P2}_1$), the constraints, such as (26b), (26c), (26d), (26e), (29b), (29c), (29d), and (29e), are the same for the effective and interference cases, with the only difference lying in the objective function (26a). In the interference case, interference originates from T_p. Therefore, $\mathcal{P}_p\left|g_{pg}\right|^2$ is the additional term in SINR. Though $\mathcal{P}_p\left|g_{pg}\right|^2$ is constant in the optimisation problem ($\mathrm{P2}_1$), the proof can be obtained following similar steps as those in the proof of **Theorem 1**. Therefore, the same optimal solutions ($\mathcal{P}_u^*$ and $\mathcal{P}_m^*$) are applied in the effective and interference cases. Based on the above discussion, the proposed transmit power allocation (TPA) algorithm can be given as algorithm TPA 1 below.

TPA 1: Maximum Energy Efficiency and Minimum Latency of mMTC/URLLC-UAV for Effective and Interference Cases

1. Initialise the parameters f_c, $\mathcal{B}$, Φ, φ, L_N, L_L, t_s, t_t, p_f, and p_d, etc;
2. For each h_a, calculate $\mathcal{P}_u^*$ and $\mathcal{P}_m^*$ based on **Theorem 1**;
3. $EE_{muE}(\mathcal{P}_u^*,\mathcal{P}_m^*) \leftarrow \mathcal{P}_u^*$ and $\mathcal{P}_m^*$;
4. $EE_{muI}(\mathcal{P}_u^*,\mathcal{P}_m^*) \leftarrow \mathcal{P}_u^*$ and $\mathcal{P}_m^*$;
5. $t_{propE}(\mathcal{P}_u^*,\mathcal{P}_m^*) \leftarrow \mathcal{P}_u^*$ and $\mathcal{P}_m^*$;
6. $t_{propI}(\mathcal{P}_u^*,\mathcal{P}_m^*) \leftarrow \mathcal{P}_u^*$ and $\mathcal{P}_m^*$;
7. Goto step (2);

V. NUMERICAL RESULTS AND DISCUSSION

In this section, we present the numerical results for evaluating the performance of the proposed UAV-assisted cognitive scheme for URLLC and mMTC services in an aerial network, as shown in Fig. 1. Based on the figure, we consider a bounded area of size $250\times600\times500$ m^3, where T_p, T_{sm}/T_{su}, and R_{sg} are located at $T_p = (10, 500, 20)$, $T_{sm}/T_{su} = (210, 215, 500)$, and $R_{sg} = (0, 0, 15)$, respectively, shown in Fig. 4. In such a network, we adopt the simulation parameters provided in Table 1. Some parameters were changed, as indicated in the figure. The pathloss is computed at 2.4 GHz operating frequency for the dense-urban scenario. For the A-t-G link, channel gain is calculated by using (2), (3), (4), and (5). For the G-t-G link, channel gain is calculated by using (2), (3), and (6).

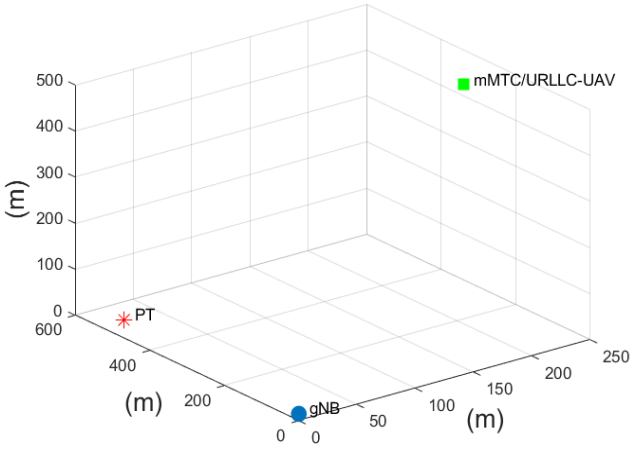

FIGURE 4. Location of gNB, PT and mMTC/URLLC-UAV.

A. IMPACT OF SIC COEFFICIENT

Fig. 5 shows the impact of SIC coefficient (Θ) on system throughput for the effective and interference cases of T_{sm}/T_{su}, respectively given in (15) and (18). It can be observed that both the system effective and interference throughput decrease w.r.t. increasing Θ for all schemes of T_{sm}/T_{su}. Now, by comparing the system effective throughput at 0.5 of Θ, we observe that the system throughput is 5.917×10^5 bps.

TABLE 1. System Parameters.

Parameter	Description	Value	Parameter	Description	Value
f_c [GHz]	Carrier frequency	2.4	$\mathcal{B}$ [MHz]	Bandwidth	1
Φ	Environment constant	12.087	φ	Environment constant	0.1139
L_L [dB]	Attenuation loss of LoS	23	L_N [dB]	Attenuation loss of NLoS	1.6
t_s [ms]	Sensing time	0.125	t_t [ms]	Transmission time	0.125
p_d	Detection probability	0.9	p_f	False alarm probability	0.1
$\rho\,[kg/m^3]$	Air density	1.225	s	Rotor solidity	0.05
$A_d\,[m^2]$	Rotor disc area	0.503	δ	Profile drag coefficient,	0.012
$v_a\,[rad/s]$	Blade angular velocity	300	$r\,[m]$	Rotor radius	0.4
η	Incremental correctional factor of induced power	0.1	W [N]	Weight of UAV	35
$\mathcal{K}$ [dB]	Rician factor	-10	N_o [dBm]	Noise power spectral density	-174
ε	Decoding error probability	10^{-7}	C_b	Channel blocklength	256
N_b	Transmitted bits	256	$\mathbb{P}_c$ [W]	Constant power consumption	1
$\mathcal{P}_u$ [W]	Transmit power of T_{su}	0.35	$\mathcal{P}_m$ [W]	Transmit power of T_{sm}	0.15
$\mathcal{P}_p$ [W]*	Transmit power of T_p	100	$\mathcal{P}_t$ [W]	Total power budget	0.5

Φ, φ, L_N, and L_L are assumed for dense-urban area.

*Here, we assume that a mobile television transmitter (Digital Video Broadcasting-Handheld) works as a T_p [41].

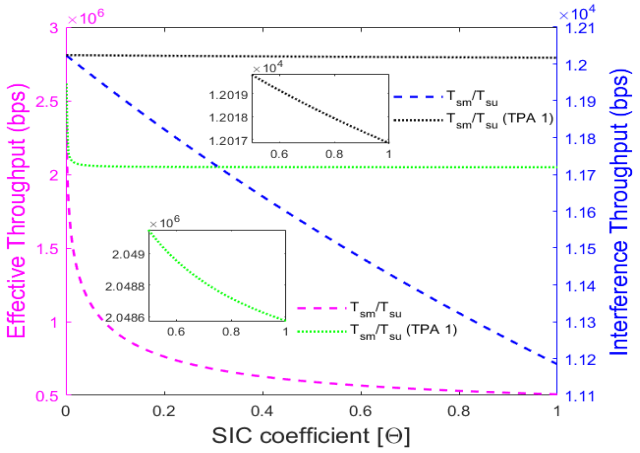

FIGURE 5. System throughput in various SIC coefficients for effective and interference cases. Setup: $p_r\,(\Omega=0)=0.5$, $p_r\,(\Omega=1)=0.5$, $h_a=500$ m, and $r_{ug}=300.5412$ m.

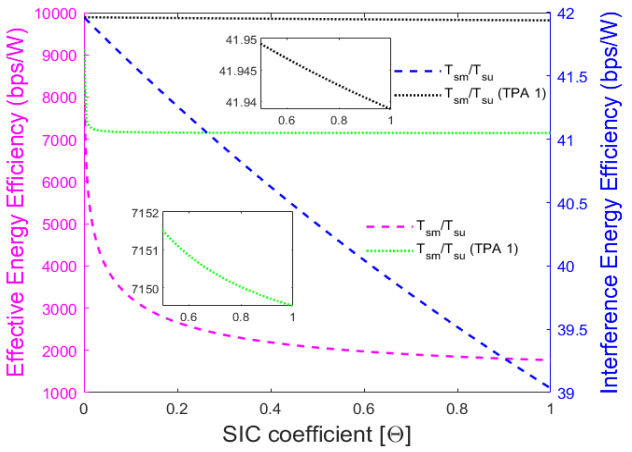

FIGURE 6. Energy efficiency in various SIC coefficients for effective and interference cases. Setup: $p_r\,(\Omega=0)=0.5$, $p_r\,(\Omega=1)=0.5$, $h_a=500$ m, and $r_{ug}=300.5412$ m.

In addition, the system effective throughput for TPA 1 is 2.049×10^6 bps. Thus, the TPA 1 algorithm improves the system effective throughput to 246.29%. On the other hand, by comparing the system interference throughput at 0.5 of Θ, we observe that the system throughput is 1.156×10^4 bps, whereas the system interference throughput for TPA 1 algorithm is 1.202×10^4 bps. Thus, the TPA 1 algorithm improves the system interference throughput to 3.9792%. It can be seen clearly that system throughput performance drops when Θ increases. This is because interference term regarding SIC operation contributes to degrade performance on system throughput. In general, SINR drops when Θ increases as given in (12).

Fig. 6 illustrates the impact of Θ on energy efficiency for the effective and interference cases of T_{sm}/T_{su} where we see that for all schemes of T_{sm}/T_{su}, both the effective and interference energy efficiency decrease w.r.t. increasing Θ. Now, by comparing the effective energy efficiency at 0.5 of Θ, we observe that the energy efficiency is 2065 bps/W. In addition, the effective energy efficiency for TPA 1 algorithm is 7152 bps/W. Thus, the TPA 1 algorithm improves the effective energy efficiency to 246.34%. On the other hand, by comparing the interference energy efficiency at 0.5 of Θ, we observe that the energy efficiency is 40.33 bps/W. Moreover, the interference energy efficiency for TPA 1 is 41.95 bps/W. Thus, the TPA 1 algorithm improves the interference energy efficiency to 4.02%. Therefore, the TPA 1 algorithm is clearly the most energy-efficient in all schemes.

Fig. 7 displays the impact of Θ on latency for the effective and interference cases of T_{sm}/T_{su}. As shown in Fig. 7,

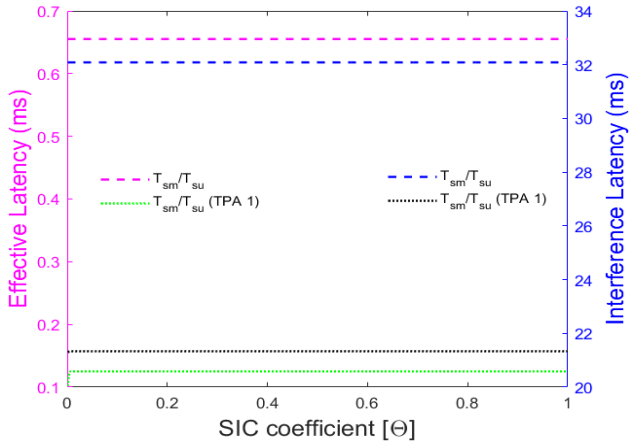

FIGURE 7. Latency in various SIC coefficients for effective and interference cases. Setup: $p_r\ (\Omega = 0) = 0.5$, $p_r\ (\Omega = 1) = 0.5$, $h_a = 500$ m, and $r_{ug} = 300.5412$ m.

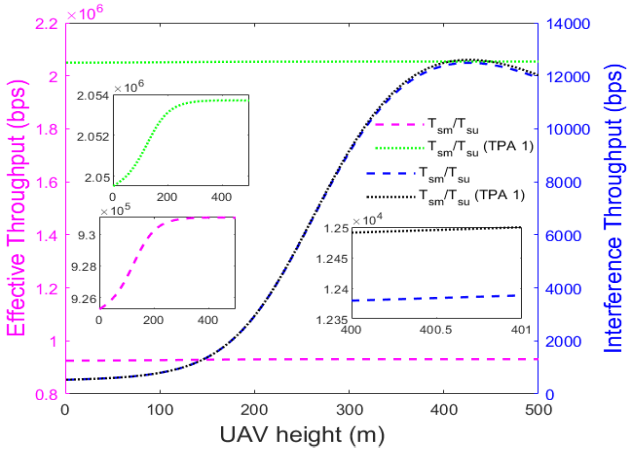

FIGURE 8. System throughput in various UAV heights for effective and interference cases. Setup: $p_r\ (\Omega = 0) = 0.5$, $p_r\ (\Omega = 1) = 0.5$, $\Theta = 0.1$, and $r_{ug} = 300.5412$ m.

as Θ increases, the latency for all schemes of T_{sm}/T_{su} becomes stable. This is because there is no relationship of Θ in SINR as given in (11). Now, by comparing the effective latency at 0.5 of Θ, we observe that the latency is 0.6551 ms whereas the latency for TPA 1 is 0.125 ms. Therefore, the TPA 1 algorithm improves the performance to 80.92% for effective case. The above results indicate that the latency requirement of our proposed model is lower than 0.125 ms. On the other hand, by comparing the interference latency at 0.5 of Θ, we observe that the latency is 32.09 ms whereas the latency for TPA 1 is 21.34 ms. Therefore, the TPA 1 algorithm improves the performance to 33.4995% for interference case. However, the proposed system model does not provide a satisfactory level of latency requirement for the interference case. This is because the interference cancellation of the PT technique is not applied here. As a result of the interference case, the latency is higher than 0.125 ms. Moreover, the trends of reduction in latency can decrease the number of transmission bits.

B. IMPACT OF UAV HEIGHT

Fig. 8 shows the impact of UAV height (h_a) on system throughput for the effective and interference cases of T_{sm}/T_{su}. As shown in Fig. 8, as h_a increases, the system throughput starts to increase and then decrease after achieving a certain h_a. This is because the LoS probability increases with h_a initially, but the LoS probability stabilises from a particular h_a. Now, by comparing the system effective throughput at 200 m, we observe that the system throughput is 9.302×10^5 bps whereas the system throughput for TPA 1 algorithm is 2.053×10^6 bps. Therefore, the TPA 1 algorithm improves the system throughput to 120.71% for effective case. On the other hand, by comparing the system interference throughput at 200 m, we observe that the system throughput is 2936 bps whereas the system throughput for TPA 1 algorithm is 2941 bps. Therefore, TPA 1 algorithm improves the system throughput to 0.1703% for interference case.

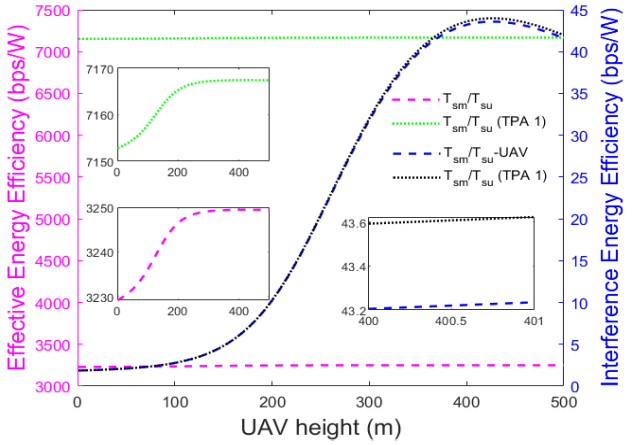

FIGURE 9. Energy efficiency in various UAV heights for effective and interference cases. Setup: $p_r\ (\Omega = 0) = 0.5$, $p_r\ (\Omega = 1) = 0.5$, $\Theta = 0.1$, and $r_{ug} = 300.5412$ m.

Fig. 9 illustrates the impact of h_a on energy efficiency for the effective and interference cases of T_{sm}/T_{su}. Here, at the beginning the energy efficiency starts to increase w.r.t. h_a and after reaching a certain h_a, the energy efficiency starts to decrease with h_a increasing. This is attributed to the use of LoS probability. Now, by comparing the effective energy efficiency at 200 m, we see that the energy efficiency is 3246 bps/W whereas the energy efficiency for TPA 1 algorithm is 7165 bps/W. Thus, the TPA 1 algorithm improves the energy efficiency to 120.733% for effective case. On the other hand, by comparing the interference energy efficiency at 200 m, we see that the energy efficiency is 10.25 bps/W. In addition, the interference energy efficiency for TPA 1 algorithm is 10.27 bps/W. Thus, the TPA 1 algorithm improves the energy efficiency to 0.1951% for interference case. Therefore, of all schemes, the TPA 1 algorithm is the most energy-efficient.

Fig. 10 presents the impact of h_a on latency for the effective and interference cases. As h_a increases, the latency decreases first and then remains constant after achieving a certain h_a.

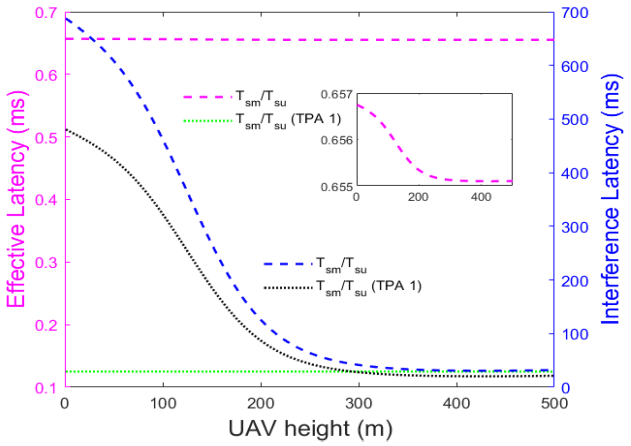

FIGURE 10. Latency in various UAV heights for effective and interference cases. Setup: $p_r\ (\Omega = 0) = 0.5$, $p_r\ (\Omega = 1) = 0.5$, $\Theta = 0.1$, and $r_{ug} = 300.5412$ m.

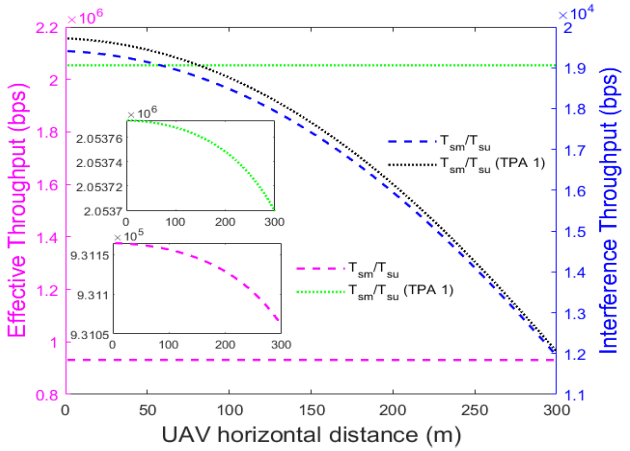

FIGURE 11. System throughput in various UAV horizontal distances for effective and interference cases. Setup: $p_r\ (\Omega = 0) = 0.5$, $p_r\ (\Omega = 1) = 0.5$, $\Theta = 0.1$, and $h_a = 500$ m.

This is attributed to the fact that the LoS probability increases with h_a initially, but becomes stable from a particular h_a. For the TPA 1 algorithm, effective latency remains constant because minimum SINR of T_{su} (v_u) is calculated by using (23) [See Appendix B]. Now, by comparing the effective latency at 200 m, we observe that the latency is 0.6553 ms whereas the latency for TPA 1 algorithm is 0.125 ms. Therefore, it is clear that the TPA 1 algorithm improves the latency to 80.9248%. The above results indicate that the latency requirement of our proposed model is lower than 0.125 ms. On the other hand, by comparing the interference latency at 200 m, we observe that the latency is 125.9 ms. Also, the interference latency for TPA 1 algorithm is 87.17 ms. Therefore, the TPA 1 algorithm improves the latency to 30.7625% for interference case.

C. IMPACT OF UAV DISTANCE

Fig. 11 shows the impact of UAV horizontal distance (r_{ug}) on system throughput for the effective and interference cases of T_{sm}/T_{su}. We see that the system throughput gradually decreases with the increasing r_{ug} for T_{sm}/T_{su}. Now, by comparing the system effective throughput at 200 m, we observe that the system throughput is 9.311×10^5 bps. In addition, the system effective throughput for TPA 1 algorithm is 2.054×10^6 bps. Thus, the TPA 1 algorithm improves the system throughput to 120.5993% for effective case. On the other hand, by comparing the system interference throughput at 200 m, we observe that the system interference throughput is 1.595×10^4 bps. Moreover, the system throughput for TPA 1 algorithm is 1.615×10^4 bps. Thus, the TPA 1 algorithm improves the system throughput to 1.2539% for interference case.

Fig. 12 presents the impact of r_{ug} on energy efficiency for the effective and interference cases of T_{sm}/T_{su}. Similar behavior is observed in Figs. 11 and 12. Now, by comparing the effective energy efficiency at 200 m, we observe that the energy efficiency is 3250 bps/W. In addition, the effective energy efficiency for TPA 1 algorithm is 7168 bps/W.

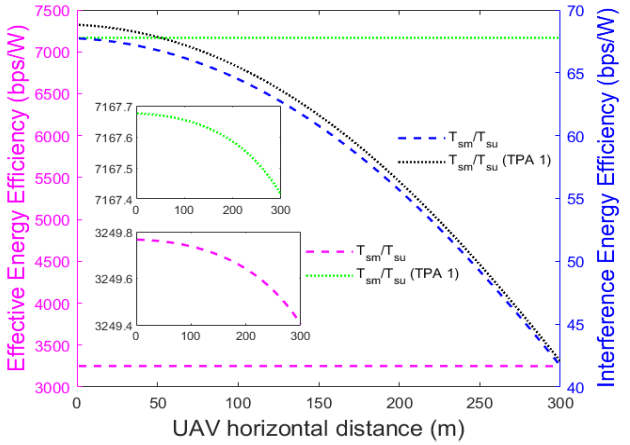

FIGURE 12. Energy efficiency in various UAV horizontal distances for effective and interference cases. Setup: $p_r\ (\Omega = 0) = 0.5$, $p_r\ (\Omega = 1) = 0.5$, $\Theta = 0.1$, and $h_a = 500$ m.

Thus, the TPA 1 algorithm improves the energy efficiency to 120.55% for effective case. On the other hand, by comparing the interference energy efficiency at 200 m, we observe that the energy efficiency is 55.67 bps/W whereas the energy efficiency for TPA 1 algorithm is 56.36 bps/W. Moreover, TPA 1 algorithm improves the energy efficiency to 1.2394% for interference case. Therefore, the TPA 1 algorithm is clearly the best in all schemes in terms of energy efficiency.

Fig. 13 illustrates the impact of r_{ug} on latency for the effective and interference cases of T_{sm}/T_{su}. We see that the latency gradually increases w.r.t. r_{ug}. This is because the latency is inversely proportional to the throughput. For the TPA 1 algorithm, effective latency remains constant. Similar behavior is observed in Figs. 10 and 13. Now, by comparing the effective latency at 200 m, we observe that the latency is 0.6551 ms whereas the latency for TPA 1 algorithm is 0.125 ms. Therefore, TPA 1 algorithm improves the latency to 80.92% for effective case. The above results indicate that

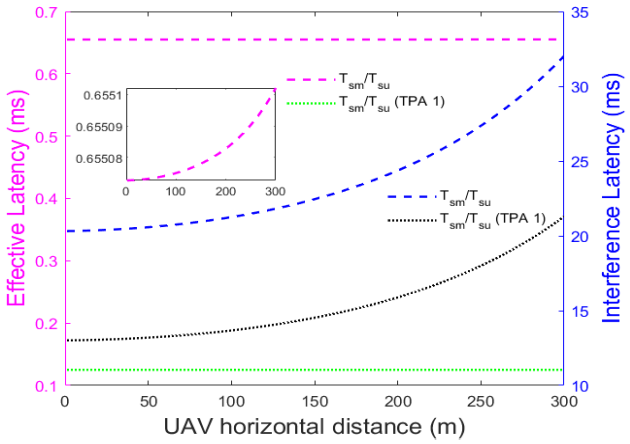

FIGURE 13. Latency in various UAV horizontal distances for effective and interference cases. Setup: $p_r\ (\Omega = 0) = 0.5$, $p_r\ (\Omega = 1) = 0.5$, $\Theta = 0.1$, and $h_a = 500$ m.

the latency requirement of our proposed model is lower than 0.125 ms. On the other hand, by comparing the interference latency at 200 m, we observe that the latency is 24.37 ms whereas the latency for TPA 1 is 15.89 ms. Thus, TPA 1 algorithm improves the latency to 34.7969% for interference case. Therefore, the TPA 1 algorithm is clearly the best in all schemes in terms of latency.

D. IMPACT OF CORRECT AND INCORRECT DETECTION PROBABILITY

Fig. 14 shows the impact of correct detection probability $\left(p_r\ (\Omega = 0)\left(1 - p_f\right)\right)$ on system throughput and energy efficiency for the effective case of T_{sm}/T_{su}. We see that for all schemes, the system effective throughput increases with $p_r\ (\Omega = 0)\left(1 - p_f\right)$ increasing. Due to the TPA 1 algorithm, system effective throughput gradually increases when $p_r\ (\Omega = 0)\left(1 - p_f\right) \leq 0.73$, after that system effective throughput sharply increases. This is because $\mathcal{P}_{u1}$ is

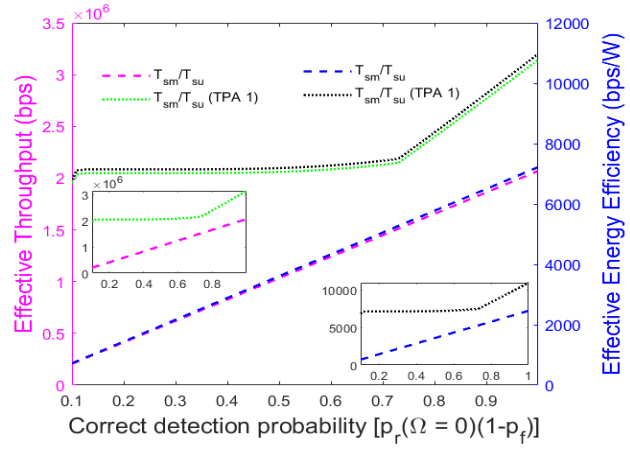

FIGURE 14. System throughput and energy efficiency in various correct detection probabilities for effective case. Setup: $r_{ug} = 300.5412$ m, $h_a = 500$ m, and $\Theta = 0.1$.

greater than $\mathcal{P}_{u2}$ when $p_r\ (\Omega = 0)\left(1 - p_f\right) \leq 0.73$. Now, by comparing the system effective throughput at 0.5 of the $p_r\ (\Omega = 0)\left(1 - p_f\right)$, we see that the system effective throughput is 1.034×10^6 bps. In addition, the system effective throughput for TPA 1 algorithm is 2.06×10^6 bps. Therefore, TPA 1 algorithm improves the system effective throughput to 99.12%. On the other hand, by comparing the energy efficiency at 0.5 of the $p_r\ (\Omega = 0)\left(1 - p_f\right)$, we observe that the energy efficiency is 3610.44 bps/W. Moreover, the energy efficiency for TPA 1 algorithm is 7189 bps/W. Thus, the TPA 1 algorithm improves the energy efficiency to 99.11%. Therefore, the TPA 1 algorithm is clearly the best in terms of energy efficiency.

Fig. 15 displays the impact of incorrect detection probability $(p_r\ (\Omega = 1)\ (1 - p_d))$ on system throughput and energy efficiency for the interference case of T_{sm}/T_{su} where we observe that for all schemes, the system interference throughput increases w.r.t. $p_r\ (\Omega = 1)\ (1 - p_d)$. Now, by comparing the system interference throughput at 0.5 of the $p_r\ (\Omega = 1)\ (1 - p_d)$, we see that the system interference throughput is 1.192×10^5 bps. In addition, the system interference throughput for TPA 1 algorithm is 1.202×10^5 bps. Therefore, TPA 1 algorithm improves the system interference throughput to 0.8389%. On the other hand, by comparing the interference energy efficiency at 0.5 of the $p_r\ (\Omega = 1)\ (1 - p_d)$, we observe that the energy efficiency is 416 bps/W. Moreover, the energy efficiency for TPA 1 algorithm is 419.6 bps/W. Thus, the TPA 1 algorithm improves the interference energy efficiency to 0.8654%.

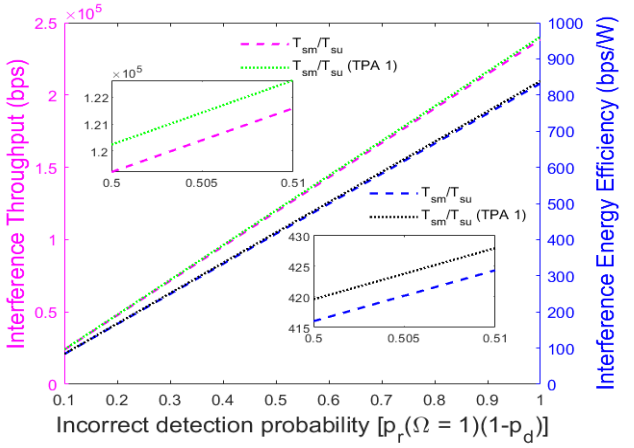

FIGURE 15. System throughput and energy efficiency in various incorrect detection probabilities for interference case. Setup: $r_{ug} = 300.5412$ m, $h_a = 500$ m, and $\Theta = 0.1$.

Fig. 16 illustrates the impact of $p_r\ (\Omega = 0)\left(1 - p_f\right)$ on latency for the effective case of T_{sm}/T_{su}. We observe that the latency decreases with the increasing $p_r\ (\Omega = 0)\left(1 - p_f\right)$. Due to the TPA 1 algorithm, effective latency decreases when $p_r\ (\Omega = 0)\left(1 - p_f\right) \geq 0.73$. This is because $\mathcal{P}_{u2}$ is greater than $\mathcal{P}_{u1}$ when $p_r\ (\Omega = 0)\left(1 - p_f\right) \geq 0.73$. Now, by comparing the latency at $0.5\ p_r\ (\Omega = 0)\left(1 - p_f\right)$, we observe that the latency is 0.589 ms whereas the latency for TPA 1 algorithm

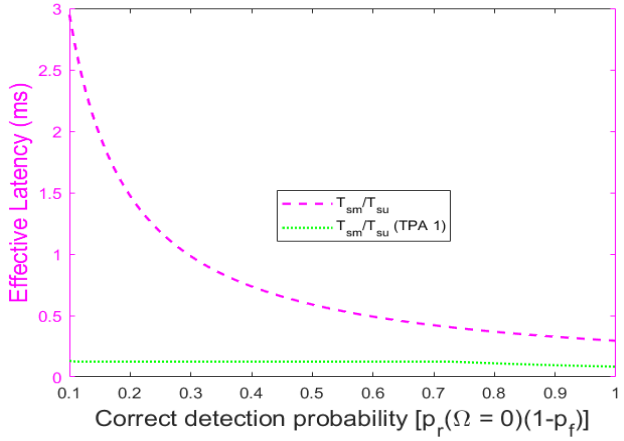

FIGURE 16. Latency in various correct detection probabilities for effective case. Setup: $r_{ug} = 300.5412$ m, $h_a = 500$ m, and $\Theta = 0.1$.

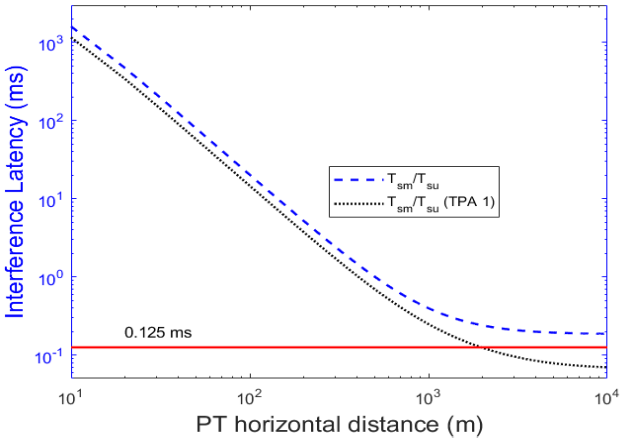

FIGURE 18. Latency in various PT horizontal distances for interference case. Setup: $r_{ug} = 300.5412$ m, $h_a = 500$ m, $N_b = 10$ bits, and $\Theta = 0.1$.

is 0.125 ms. Thus, the TPA 1 algorithm improves the latency to 78.77%. Therefore, the TPA 1 algorithm is clearly the best in all schemes in terms of latency.

Fig. 17 displays the impact of $p_r\,(\Omega = 1)\,(1 - p_d)$ on latency for the interference case of T_{sm}/T_{su}. We see that the latency decreases w.r.t. $p_r\,(\Omega = 1)\,(1 - p_d)$. Now, by comparing the latency at $0.5\,p_r\,(\Omega = 1)\,(1 - p_d)$, we see that the latency is 3.20 ms whereas the latency for TPA 1 of T_{su} and T_{sm} is 2.134 ms. Thus, TPA 1 algorithm improves the latency to 33.31% for incorrect detection probability.

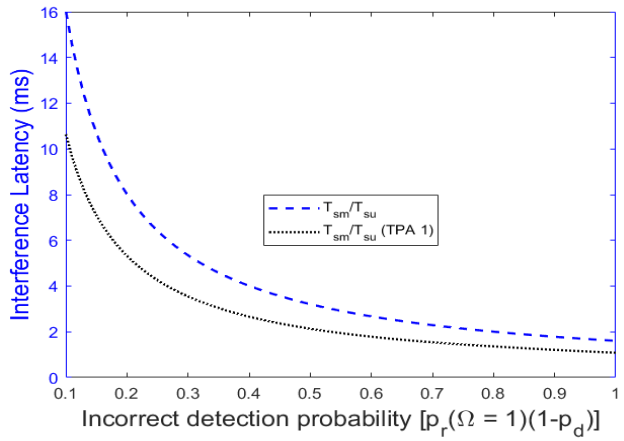

FIGURE 17. Latency in various incorrect detection probabilities for interference case. Setup: $r_{ug} = 300.5412$ m, $h_a = 500$ m, and $\Theta = 0.1$.

E. IMPROVEMENT OF INTERFERENCE LATENCY

Fig. 18 illustrates the impact of PT horizontal distance on latency for the interference case of T_{sm}/T_{su}. We observe that the latency decreases with the increasing PT horizontal distance. It can be observed that interference latency is lower than 0.125 ms when the distance of PT is far 1974 m from the gNB. Also, it can be seen that the TPA 1 algorithm is clearly the best in all schemes in terms of latency.

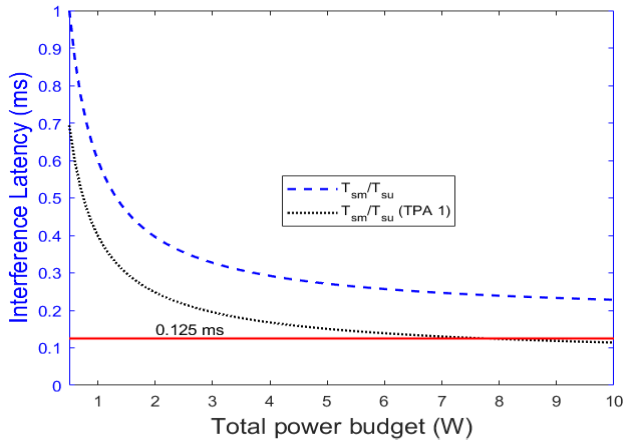

FIGURE 19. Latency in various total power budgets for interference case. Setup: $r_{ug} = 300.5412$ m, $h_a = 500$ m, $N_b = 10$ bits, and $\Theta = 0.1$.

Fig. 19 displays the impact of total power budget on latency for the interference case of T_{sm}/T_{su}. We see that the latency decreases w.r.t. the increasing total power budget. It can be observed that interference latency is lower than 0.125 ms when the total power budget is higher than 7.78 W. Now, by comparing the latency at 5 W, we see that the latency is 0.2711 ms whereas the latency for TPA 1 algorithm is 0.1507 ms. Thus, TPA 1 algorithm improves the latency to 32.444% for total power budget scheme.

F. COMPARISON WITH TPA 1 ALGORITHM FOR EFFECTIVE AND INTERFERENCE CASES

From the Table 2 and Figs. 18-19, several key points can be presented based on the application of the proposed model:

- In case of energy efficiency using TPA 1 algorithm, the improvements in energy efficiency are 99.11% for the effective case and 0.86% for the interference case. Thus, the TPA 1 algorithm achieves better energy efficiency.
- In case of latency using TPA 1 algorithm, the improvements in latency are 78.77% for the effective case and

TABLE 2. Comparisons of TPA 1 algorithm for effective and interference cases of mMTC/URLLC-UAV device for correct and incorrect detection probability at 0.5 in terms of throughput, energy efficiency, and latency.

Cases	Performance Metrics	Original	TPA 1	Improvement (⇑) of TPA 1 compared with Original
Effective mMTC/URLLC-UAV	Throughput (bps)	1.034×10^6	2.06×10^6	99.12% (⇑)
Interference mMTC/URLLC-UAV	Throughput (bps)	1.192×10^5	1.202×10^5	0.83% (⇑)
Effective mMTC/URLLC-UAV	Energy efficiency (bps/W)	3610.44	7189	99.11% (⇑)
Interference mMTC/URLLC-UAV	Energy efficiency (bps/W)	416	419.6	0.86% (⇑)
Effective mMTC/URLLC-UAV	Latency (ms)	0.589	0.125	78.77% (⇑)
Interference mMTC/URLLC-UAV	Latency (ms)	3.20	2.13	33.31% (⇑)

33.31% for the interference case. Even though both cases improve latency, the TPA 1 algorithm fulfils the latency requirement for the effective case, but not for the interference case.

- In case of interference latency using TPA 1 algorithm, it is possible to fulfill the latency requirement of 0.125 ms, numerical analysis of Figs. 18 and 19 confirms that (i) the number of transmitting bits is reduced, (ii) the distance between PT and gNB is increased, and (iii) the total power budget is increased.

VI. CONCLUSION

This paper focuses on analyzing a cognitive UAV wireless network based on NOMA transmission for URLLC and mMTC services, where a secondary mMTC/URLLC-UAV transmitter sends information to a ground gNB in the presence of PT. For the considered NOMA system, we derive the expressions of throughput, energy efficiency, and latency for mMTC/URLLC-UAV device. Then, we aim at maximising the energy efficiency and minimising the latency of the mMTC/URLLC-UAV device by jointly optimising the transmission power of mMTC and URLLC users. Theoretical derivations and numerical results show that the proposed scheme achieves a higher energy efficiency for the mMTC/URLLC-UAV device. Moreover, it is shown that the improvement of latency is achieved for the effective case. In future work, we will investigate the energy harvesting technique [33], transmit antenna selection technique [42], network coding scheme [43], and sub-terahertz communication [44] in a UAV-aided spectrum sensing CR network.

APPENDIX A
PROOF OF EFFECTIVE CASE THROUGHPUT

As stated in [45], the effective throughput for IBL information theoretic model when $\Omega = 0$ can be expressed as

$$ED = \frac{t_t}{t_s + t_t} p_r\left(\Omega = 0\right)\left(1 - p_f\right)\log_2\left(1 + \text{SINR}\right). \quad \text{(A.1)}$$

Referring in [45], the interference throughput for IBL information theoretic model when $\Omega = 1$ can be expressed as

$$ID = \frac{t_t}{t_s + t_t} p_r\left(\Omega = 1\right)\left(1 - p_d\right)\log_2\left(1 + \text{SINR}\right). \quad \text{(A.2)}$$

From (A.1) and (A.2), it is reformulated for FBL information theoretic model. For the effective and interference cases, (A.1) and (A.2) are same for T_{su} and T_{sm}, however SINR is different for T_{su} and T_{sm}. The expression of SINR is provided in (11) and (12).

APPENDIX B
PROOF OF EFFECTIVE CASE LATENCY

According to the assumption of (26a and 19), the Hessian matrix of objective function is written as

$$\nabla^2 EE_{muE}(\mathcal{P}_u, \mathcal{P}_m) = \begin{bmatrix} \frac{\partial^2 EE_{muE}(\mathcal{P}_u, \mathcal{P}_m)}{\partial \mathcal{P}_u^2} & \frac{\partial^2 EE_{muE}(\mathcal{P}_u, \mathcal{P}_m)}{\partial \mathcal{P}_u \partial \mathcal{P}_m} \\ \frac{\partial^2 EE_{muE}(\mathcal{P}_u, \mathcal{P}_m)}{\partial \mathcal{P}_m \partial \mathcal{P}_u} & \frac{\partial^2 EE_{muE}(\mathcal{P}_u, \mathcal{P}_m)}{\partial \mathcal{P}_m^2} \end{bmatrix} \quad \text{(B.1)}$$

It is observed that (B.1) is negative. Hence, the optimization problem ($P1_2$) is non-convex. Now, we find the minimum SINR requirement of T_{su} and T_{sm} using (13) and (14). From (23), we get

$$ED_u = 8000 N_b. \quad \text{(B.2)}$$

Substituting ED_u into (13) and then rearranging the equation, we obtain an equivalent representation of (13) and (14) as follows

$$\mathcal{B}\log_2\left(1 + \upsilon_u\right) - \sqrt{\frac{\upsilon_u^0}{C_b}} Q_{in} - \frac{8000\, N_b}{t_1} = 0, \quad \text{(B.3)}$$

$$\mathcal{B}\log_2\left(1 + \upsilon_m\right) - \sqrt{\frac{\upsilon_m^0}{C_b}} Q_{in} - \frac{ED_m}{t_1} = 0, \quad \text{(B.4)}$$

where $t_1 = \frac{t_t}{t_s + t_t} p_r\left(\Omega = 0\right)\left(1 - p_f\right)$, $\upsilon_u^0 = 1 - (1 + \upsilon_u)^{-2}$, $\upsilon_m^0 = 1 - (1 + \upsilon_m)^{-2}$, and $Q_{in} = Q^{-1}(\varepsilon)$. The system expression (B.3) and (B.4) are natural logarithm functions. Using the *vpasolve* function in MATLAB software [46], (B.3) and (B.4) can be solved. For high SINR, $\upsilon_u^0 = 1$ and $\upsilon_m^0 = 1$. After some manipulations, we obtain an equivalent representation of (B.3) and (B.4) due to high SINR as follows

$$\upsilon_u = 2^{\frac{1}{\mathcal{B}}\left\{\sqrt{\frac{1}{C_b}} Q_{in} + \frac{8000\, N_b}{t_1}\right\}} - 1. \quad \text{(B.5)}$$

$$\upsilon_m = 2^{\frac{1}{\mathcal{B}}\left\{\sqrt{\frac{1}{C_b}} Q_{in} + \frac{ED_m}{t_1}\right\}} - 1. \quad \text{(B.6)}$$

For the optimization problem ($P1_2$), the Lagrangian can be expressed as

$$\begin{aligned}\mathcal{L}(\mathcal{P}_u, \mathcal{P}_m) = EE_{muE}(\mathcal{P}_u, \mathcal{P}_m) + \delta_1 \left[\mathcal{P}_u + \mathcal{P}_m - \mathcal{P}_t\right] \\ + \delta_2 \left[\upsilon_u \left(\sigma^2 + \mathcal{P}_m \left|g_{ug}\right|^2\right) / \left|g_{ug}\right|^2 - \mathcal{P}_u\right] \\ + \delta_3 \left[\mathcal{P}_u - (\mathcal{P}_m/\Theta\upsilon_m) + \left(\sigma^2/\Theta \left|g_{ug}\right|^2\right)\right] \\ + \delta_4 \left[\upsilon_m - \upsilon_u\right], \end{aligned} \tag{B.7}$$

where δ_1, δ_2, δ_3 and δ_4 are the Lagrangian multipliers. The first derivative of (B.7) w.r.t. $\mathcal{P}_u$ and $\mathcal{P}_m$ can be written as

$$\frac{d\mathcal{L}(\mathcal{P}_u, \mathcal{P}_m)}{d\mathcal{P}_u} = \delta_1 - \delta_2 + \delta_3 - \frac{t_1(\kappa_2 - \kappa_3)}{\kappa_1} + \frac{t_1(\kappa_4 + \kappa_5)}{\kappa_1^2}, \tag{B.8}$$

$$\begin{aligned}\frac{d\mathcal{L}(\mathcal{P}_u, \mathcal{P}_m)}{d\mathcal{P}_m} = \delta_1 + \delta_2\upsilon_u - \frac{\delta_3}{\upsilon_m\Theta} + \frac{t_1(\kappa_6 - \kappa_7)}{\kappa_1} \\ + \frac{t_1(\kappa_4 + \kappa_5)}{\kappa_1^2}, \end{aligned} \tag{B.9}$$

where $l = \left|g_{ug}\right|^2$, $\kappa_1 = P_{hov} + \mathcal{P}_u + \mathcal{P}_m + \mathbb{P}_c$, $\kappa_2 = \frac{\mathcal{B}\mathcal{P}_m l^2 Q_{in}}{c_2 c_1^2 \log(2)} - \frac{\mathcal{P}_m l^2 Q_{in}\Theta}{c_4 c_2^3 c_1^2 C_b}$, $\kappa_3 = \frac{\mathcal{B}l}{c_3(\sigma^2+\mathcal{P}_m l)\log(2)} - \frac{lQ_{in}}{c_5 c_3^3(\sigma^2+\mathcal{P}_m l)C_b}$, $\kappa_4 = c_4 Q_{in} - \frac{\mathcal{B}\log(c_2)}{\log(2)}$, $\kappa_5 = c_5 Q_{in} - \frac{\mathcal{B}\log(c_3)}{\log(2)}$, $\kappa_6 = \frac{\mathcal{B}l}{c_2 c_1 \log(2)} - \frac{lQ_{in}}{c_4 c_2^3 c_1 C_b}$, $\kappa_7 = \frac{\mathcal{B}\mathcal{P}_u l^2}{c_3 c_6 \log(2)} - \frac{\mathcal{P}_u l^2 Q_{in}}{c_5 c_6 c_3^3 C_b}$, $c_1 = \sigma^2 + \Theta\mathcal{P}_u l$, $c_2 = 1 + \frac{\mathcal{P}_m l}{c_1}$, $c_3 = 1 + \frac{\mathcal{P}_u l}{\sigma^2+\mathcal{P}_m l}$, $c_4 = \sqrt{-\frac{\frac{1}{c_2^2}-1}{C_b}}$, $c_5 = \sqrt{-\frac{\frac{1}{c_3^2}-1}{C_b}}$, and $c_6 = (\sigma^2 + \mathcal{P}_m l)^2$.

According to the theory of KKT, KKT conditions are necessary and sufficient to obtain optimal solutions, so we can write KKT conditions as follows:

$$\begin{cases} \delta_1 \geq 0, \delta_2 \geq 0, \delta_3 \geq 0, \delta_4 \geq 0 \\ \delta_1 \left[\mathcal{P}_u + \mathcal{P}_m - \mathcal{P}_t\right] = 0 \\ \delta_2 \left[\upsilon_u \left(\sigma^2 + \mathcal{P}_m l\right)/l - \mathcal{P}_u\right] = 0 \\ \delta_3 \left[\mathcal{P}_u - (\mathcal{P}_m/\Theta\upsilon_m) + \left(\sigma^2/\Theta l\right)\right] = 0 \\ \delta_4 \left[\upsilon_m - \upsilon_u\right] = 0 \\ \dfrac{d\mathcal{L}(\mathcal{P}_u, \mathcal{P}_m)}{d\mathcal{P}_u} = 0, \quad \frac{d\mathcal{L}(\mathcal{P}_u, \mathcal{P}_m)}{d\mathcal{P}_m} = 0 \\ \mathcal{P}_u \geq 0, \quad \mathcal{P}_m \geq 0. \end{cases} \tag{B.10}$$

From the aforementioned conditions, we find the optimal solutions for the following expressions as follows

$$\mathcal{P}_u + \mathcal{P}_m - \mathcal{P}_t = 0. \tag{B.11}$$

$$\upsilon_u \left(\sigma^2 + \mathcal{P}_m l\right)/l - \mathcal{P}_u = 0. \tag{B.12}$$

$$\mathcal{P}_u - (\mathcal{P}_m/\Theta\upsilon_m) + \left(\sigma^2/\Theta l\right) = 0. \tag{B.13}$$

Plugging the value of $\mathcal{P}_m = \mathcal{P}_t - \mathcal{P}_u$ into (B.12) and (B.13), the expressions (B.12) and (B.13) can be reduced as

$$\mathcal{P}_{u1} = \frac{\upsilon_u}{1+\upsilon_u}\left[\mathcal{P}_t + \frac{\sigma^2}{l}\right]. \tag{B.14}$$

$$\mathcal{P}_{u2} = \frac{\upsilon_m}{1+\Theta\upsilon_m}\left[\frac{\mathcal{P}_t}{\upsilon_m} - \frac{\sigma^2}{l}\right]. \tag{B.15}$$

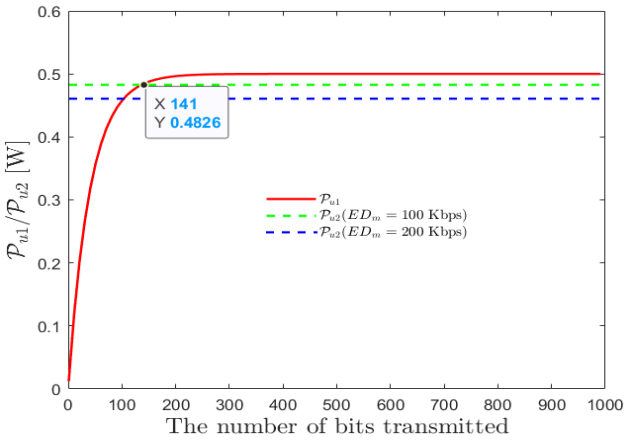

FIGURE 20. $\mathcal{P}_{u1}$ and $\mathcal{P}_{u2}$ versus the number of bits transmitted.

Fig. 20 shows that the $\mathcal{P}_{u1}$ and $\mathcal{P}_{u2}$ versus the number of bits transmitted (N_b) considering the same value given in Table 1. As can be seen in Fig. 20, $\mathcal{P}_{u1}$ increases with N_b. $\mathcal{P}_{u1}$ is lower than $\mathcal{P}_{u2}$ when $N_b \leq 131$. Thus, the optimal solution of $\mathcal{P}_u^*$ from (B.14) and (B.15) can be written as

$$\mathcal{P}_u^* = \max\left(\mathcal{P}_{u1}, \mathcal{P}_{u2}\right). \tag{B.16}$$

Substituting (B.16) into (B.11), the optimal solution of $\mathcal{P}_m^*$ can be written as

$$\mathcal{P}_m^* = \mathcal{P}_t - \mathcal{P}_u^*. \tag{B.17}$$

REFERENCES

[1] O. Liberg, M. Sundberg, E. Wang, J. Bergman, J. Sachs, and G. Wikström, *Cellular Internet of Things: From Massive Deployments to Critical 5G Applications*. New York, NY, USA: Academic, 2019.

[2] N. H. Mahmood *et al.*, "White paper on critical and massive machine type communication towards 6G," 2020, *arXiv:2004.14146*. [Online]. Available: http://arxiv.org/abs/2004.14146

[3] S. Lagen, L. Giupponi, S. Goyal, N. Patriciello, B. Bojovic, A. Demir, and M. Beluri, "New radio beam-based access to unlicensed spectrum: Design challenges and solutions," *IEEE Commun. Surveys Tuts.*, vol. 22, no. 1, pp. 8–37, 1st Quart., 2020.

[4] R. Bajracharya, R. Shrestha, and H. Jung, "Future is unlicensed: Private 5G unlicensed network for connecting industries of future," *Sensors*, vol. 20, no. 10, p. 2774, May 2020.

[5] *Technical Specification Group Radio Access Network; Study on Licensed-Assisted Access to Unlicensed Spectrum (Release 13)*, document 36.889, 3GPP, 2017.

[6] H.-J. Kwon, J. Jeon, A. Bhorkar, Q. Ye, H. Harada, Y. Jiang, L. Liu, S. Nagata, B. L. Ng, T. Novlan, J. Oh, and W. Yi, "Licensed-assisted access to unlicensed spectrum in LTE release 13," *IEEE Commun. Mag.*, vol. 55, no. 2, pp. 201–207, Feb. 2017.

[7] S. Haykin, D. J. Thomson, and J. H. Reed, "Spectrum sensing for cognitive radio," *Proc. IEEE*, vol. 97, no. 5, pp. 849–877, May 2009.

[8] *Technical Specification Group Radio Access Network; Study on Enhanced LTE Support for Aerial Vehicles (Release 15)*, document 36.777, 3GPP, 2017.

[9] Z. Ullah, F. Al-Turjman, and L. Mostarda, "Cognition in UAV-aided 5G and beyond communications: A survey," *IEEE Trans. Cognit. Commun. Netw.*, vol. 6, no. 3, pp. 872–891, Sep. 2020.

[10] H. Shakhatreh, A. H. Sawalmeh, A. Al-Fuqaha, Z. Dou, E. Almaita, I. Khalil, N. S. Othman, A. Khreishah, and M. Guizani, "Unmanned aerial vehicles (UAVs): A survey on civil applications and key research challenges," *IEEE Access*, vol. 7, pp. 48572–48634, 2019.

[11] S. Sekander, H. Tabassum, and E. Hossain, "On the performance of renewable energy-powered UAV-assisted wireless communications," 2019, *arXiv:1907.07158*. [Online]. Available: http://arxiv.org/abs/1907.07158
[12] A. Fotouhi, H. Qiang, M. Ding, M. Hassan, L. G. Giordano, A. Garcia-Rodriguez, and J. Yuan, "Survey on UAV cellular communications: Practical aspects, standardization advancements, regulation, and security challenges," *IEEE Commun. Surveys Tuts.*, vol. 21, no. 4, pp. 3417–3442, 4th Quart., 2019.
[13] B. Li, Z. Fei, and Y. Zhang, "UAV communications for 5G and beyond: Recent advances and future trends," *IEEE Internet Things J.*, vol. 6, no. 2, pp. 2241–2263, Apr. 2019.
[14] Z. H. E. Tan, A. S. Madhukumar, R. P. Sirigina, and A. K. Krishna, "Addressing spectrum efficiency through hybrid-duplex UAV communications: Challenges and opportunities," *Veh. Commun.*, vol. 24, Aug. 2020, Art. no. 100235.
[15] V. Sharma, F. Song, I. You, and M. Atiquzzaman, "Energy efficient device discovery for reliable communication in 5G-based IoT and BSNs using unmanned aerial vehicles," *J. Netw. Comput. Appl.*, vol. 97, pp. 79–95, Nov. 2017.
[16] G. Ding, Q. Wu, L. Zhang, Y. Lin, T. A. Tsiftsis, and Y.-D. Yao, "An amateur drone surveillance system based on the cognitive Internet of Things," *IEEE Commun. Mag.*, vol. 56, no. 1, pp. 29–35, Jan. 2018.
[17] Y. Liu, H.-N. Dai, H. Wang, M. Imran, X. Wang, and M. Shoaib, "UAV-enabled data acquisition scheme with directional wireless energy transfer for Internet of Things," *Comput. Commun.*, vol. 155, pp. 184–196, Apr. 2020.
[18] B. Ji, Y. Li, D. Cao, C. Li, S. Mumtaz, and D. Wang, "Secrecy performance analysis of UAV assisted relay transmission for cognitive network with energy harvesting," *IEEE Trans. Veh. Technol.*, vol. 69, no. 7, pp. 7404–7415, Jul. 2020.
[19] X. Mu, Y. Liu, L. Guo, and J. Lin, "Non-orthogonal multiple access for air-to-ground communication," *IEEE Trans. Commun.*, vol. 68, no. 5, pp. 2934–2949, May 2020.
[20] X. Zhang, J. Zhang, J. Xiong, L. Zhou, and J. Wei, "Energy-efficient multi-UAV-enabled multiaccess edge computing incorporating NOMA," *IEEE Internet Things J.*, vol. 7, no. 6, pp. 5613–5627, Jun. 2020.
[21] X. Liu, H. Ding, X. Zhang, P. Li, and C. Wu, "Rate satisfaction-based power allocation for NOMA-based cognitive Internet of Things," *Ad Hoc Netw.*, vol. 98, Mar. 2020, Art. no. 102063.
[22] M. Mozaffari, W. Saad, M. Bennis, and M. Debbah, "Mobile Internet of Things: Can UAVs provide an energy-efficient mobile architecture?" in *Proc. IEEE Global Commun. Conf. (GLOBECOM)*, Dec. 2016, pp. 1–6.
[23] M. Liu, J. Yang, and G. Gui, "DSF-NOMA: UAV-assisted emergency communication technology in a heterogeneous Internet of Things," *IEEE Internet Things J.*, vol. 6, no. 3, pp. 5508–5519, Jun. 2019.
[24] A. M. Almasoud and A. E. Kamal, "Data dissemination in IoT using a cognitive UAV," *IEEE Trans. Cognit. Commun. Netw.*, vol. 5, no. 4, pp. 849–862, Dec. 2019.
[25] G. Hattab and D. Cabric, "Energy-efficient massive IoT shared spectrum access over UAV-enabled cellular networks," *IEEE Trans. Commun.*, vol. 68, no. 9, pp. 5633–5648, Sep. 2020.
[26] Y. Hu, G. Sun, G. Zhang, M. Cenk Gursoy, and A. Schmeink, "Optimal resource allocation in ground wireless networks supporting unmanned aerial vehicle transmissions," 2020, *arXiv:2001.06850*. [Online]. Available: http://arxiv.org/abs/2001.06850
[27] C. She, C. Liu, T. Q. S. Quek, C. Yang, and Y. Li, "Ultra-reliable and low-latency communications in unmanned aerial vehicle communication systems," *IEEE Trans. Commun.*, vol. 67, no. 5, pp. 3768–3781, May 2019.
[28] C. Pan, H. Ren, Y. Deng, M. Elkashlan, and A. Nallanathan, "Joint blocklength and location optimization for URLLC-enabled UAV relay systems," *IEEE Commun. Lett.*, vol. 23, no. 3, pp. 498–501, Mar. 2019.
[29] A. Han, T. Lv, and X. Zhang, "UAV beamwidth design for ultra-reliable and low-latency communications with NOMA," in *Proc. IEEE Int. Conf. Commun. Workshops (ICC Workshops)*, May 2019, pp. 1–6.
[30] H. Ren, C. Pan, K. Wang, Y. Deng, M. Elkashlan, and A. Nallanathan, "Achievable data rate for URLLC-enabled UAV systems with 3-D channel model," *IEEE Wireless Commun. Lett.*, vol. 8, no. 6, pp. 1587–1590, Dec. 2019.
[31] Z. Chu, W. Hao, P. Xiao, and J. Shi, "UAV assisted spectrum sharing ultra-reliable and low-latency communications," in *Proc. IEEE Global Commun. Conf. (GLOBECOM)*, Dec. 2019, pp. 1–6.
[32] R. Kassab, O. Simeone, P. Popovski, and T. Islam, "Non-orthogonal multiplexing of ultra-reliable and broadband services in fog-radio architectures," *IEEE Access*, vol. 7, pp. 13035–13049, 2019.
[33] S. R. Sabuj and M. Hamamura, "Two-slope path-loss design of energy harvesting in random cognitive radio networks," *Comput. Netw.*, vol. 142, pp. 128–141, Sep. 2018.
[34] L. Sboui, H. Ghazzai, Z. Rezki, and M.-S. Alouini, "Achievable rates of UAV-relayed cooperative cognitive radio MIMO systems," *IEEE Access*, vol. 5, pp. 5190–5204, 2017.
[35] A. R. Rahul, S. R. Sabuj, M. S. Akbar, H.-S. Jo, and M. A. Hossain, "An optimization based approach to enhance the throughput and energy efficiency for cognitive unmanned aerial vehicle networks," *Wireless Netw.*, pp. 1–19, Sep. 2020.
[36] A. Al-Hourani, S. Kandeepan, and S. Lardner, "Optimal LAP altitude for maximum coverage," *IEEE Wireless Commun. Lett.*, vol. 3, no. 6, pp. 569–572, Dec. 2014.
[37] Y. Zeng, J. Xu, and R. Zhang, "Energy minimization for wireless communication with rotary-wing UAV," *IEEE Trans. Wireless Commun.*, vol. 18, no. 4, pp. 2329–2345, Apr. 2019.
[38] N. Huda Mahmood, A. Karimi, G. Berardinelli, K. I. Pedersen, and D. Laselva, "On the resource utilization of multi-connectivity transmission for URLLC services in 5G new radio," 2019, *arXiv:1904.07963*. [Online]. Available: http://arxiv.org/abs/1904.07963
[39] D.-T. Do and T.-T.-T. Nguyen, "Exploiting system performance in AF non-orthogonal multiple access network under impacts of imperfect SIC and imperfect hardware," *Phys. Commun.*, vol. 38, Feb. 2020, Art. no. 100912.
[40] F. Kara and H. Kaya, "Improved user fairness in decode-forward relaying non-orthogonal multiple access schemes with imperfect SIC and CSI," *IEEE Access*, vol. 8, pp. 97540–97556, 2020.
[41] Y. Zhang, C. Zhang, J. Cosmas, K.-K. Loo, T. Owens, R. Di Bari, Y. Lostanlen, and M. Bard, "Analysis of DVB-H network coverage with the application of transmit diversity," *IEEE Trans. Broadcast.*, vol. 54, no. 3, pp. 568–577, Sep. 2008.
[42] M. Khan, M. T. Rahman, and S. Rahman Sabuj, "A transmit antenna selection technique in random cognitive radio network," in *Proc. IEEE Region 10 Conf. (TENCON)*, Oct. 2018, pp. 0264–0267.
[43] N. Qi, M. Xiao, T. A. Tsiftsis, R. Yao, and S. Mumtaz, "Energy efficient two-tier network-coded relaying systems considering processing energy costs," *IEEE Trans. Veh. Technol.*, vol. 68, no. 1, pp. 999–1003, Jan. 2019.
[44] S. R. Sabuj, A. M. M. S. Khan, and M. Hamamura, "Application of non-orthogonal multiple access for machine type communication in subterahertz band," *Comput. Netw.*, vol. 182, Dec. 2020, Art. no. 107508.
[45] X. Liu, M. Guan, X. Zhang, and H. Ding, "Spectrum sensing optimization in an UAV-based cognitive radio," *IEEE Access*, vol. 6, pp. 44002–44009, 2018.
[46] The Mathworks. (2020). *MATLAB Symbolic Math Toolbox*. [Online]. Available: https://kr.mathworks.com/help/symbolic/solve.html

SAIFUR RAHMAN SABUJ (Member, IEEE) was born in Bangladesh. He received the B.Sc. degree in electrical, electronic, and communication engineering from Dhaka University, Bangladesh, in 2007, the M.Sc. degree in engineering from the Institute of Information and Communication Technology, Bangladesh University of Engineering and Technology, Bangladesh, in 2011, and the Ph.D. degree from the Graduate School of Engineering, Kochi University of Technology, Japan, in 2017.

From 2008 to 2013, he was a Faculty Member of Green University of Bangladesh, Metropolitan University, Sylhet, and Bangladesh University. He is currently working with the Department of Electronics and Control Engineering, Hanbat National University, South Korea, as a Postdoctoral Research Fellow. He has been an Assistant Professor with the Department of Electrical and Electronic Engineering, Brac University, Bangladesh, since September 2017. His research interests include MIMO-OFDM/NOMA, cooperative communication, cognitive radio, the Internet of Things, unmanned aerial vehicle, and machine-to-machine for wireless communications.

AZMIR AHMED received the B.Sc. degree in electronic and communication engineering from Brac University, Bangladesh, in 2019. His research interests include wireless networks, cognitive radio networks, the Internet of Things, UAV communication, 5G, and massive MIMO systems.

YEONGI CHO (Student Member, IEEE) received the B.S. and M.S. degrees in electronics and control engineering from Hanbat National University, Daejeon, South Korea, in 2018 and 2020, respectively, where he is currently pursuing the Ph.D. degree with the Department of Electronics and Control Engineering. His current research interests include the interference analysis between wireless cellular and satellite service, and wireless communication system structure (physical layer and channel modeling).

KYOUNG-JAE LEE (Senior Member, IEEE) received the B.S. and Ph.D. degrees in electrical engineering from Korea University, Seoul, South Korea, in 2005 and 2011, respectively. He was an Intern with Beceem Communications, Inc., Santa Clara, CA, USA, in 2007, and he was a Visiting Student with the University of Southern California, Los Angeles, CA, USA, in 2009. He was a Research Professor with Korea University, in 2011. From 2011 to 2012, he was a Postdoctoral Fellow with the Wireless Networking and Communications Group, The University of Texas at Austin, Austin, TX, USA. Since 2012, he has been with Hanbat National University, Daejeon, South Korea, where he is currently an Associate Professor with the Department of Electronics and Control Engineering. His research interests include communication theory, signal processing, and information theory applied to the next-generation wireless communications. He received the Best Paper Award at the IEEE VTC Fall, in 2009, the IEEE ComSoc APB Outstanding Paper Award, in 2013, and the IEEE ComSoc APB Outstanding Young Researcher Award, in 2013.

HAN-SHIN JO (Member, IEEE) received the B.S., M.S., and Ph.D. degrees in electrical and electronics engineering from Yonsei University, Seoul, South Korea, in 2001, 2004, and 2009, respectively. He is currently an Associate Professor with the Department of Electronics and Control Engineering, Hanbat National University, Daejeon, South Korea. He was a Postdoctoral Research Fellow with the Wireless Networking and Communications Group, Department of Electrical and Computer Engineering, The University of Texas at Austin, from 2009 to 2011. He developed a long-term evolution base station at Samsung Electronics, from 2011 to 2012. His current research interests include coexistence study and spectrum sharing, and applications of stochastic geometry, optimization theory, machine/reinforcement learning to wireless communications, and networking. He has been a member of Korea ITU-R Working Party 5D Committee, since 2016.